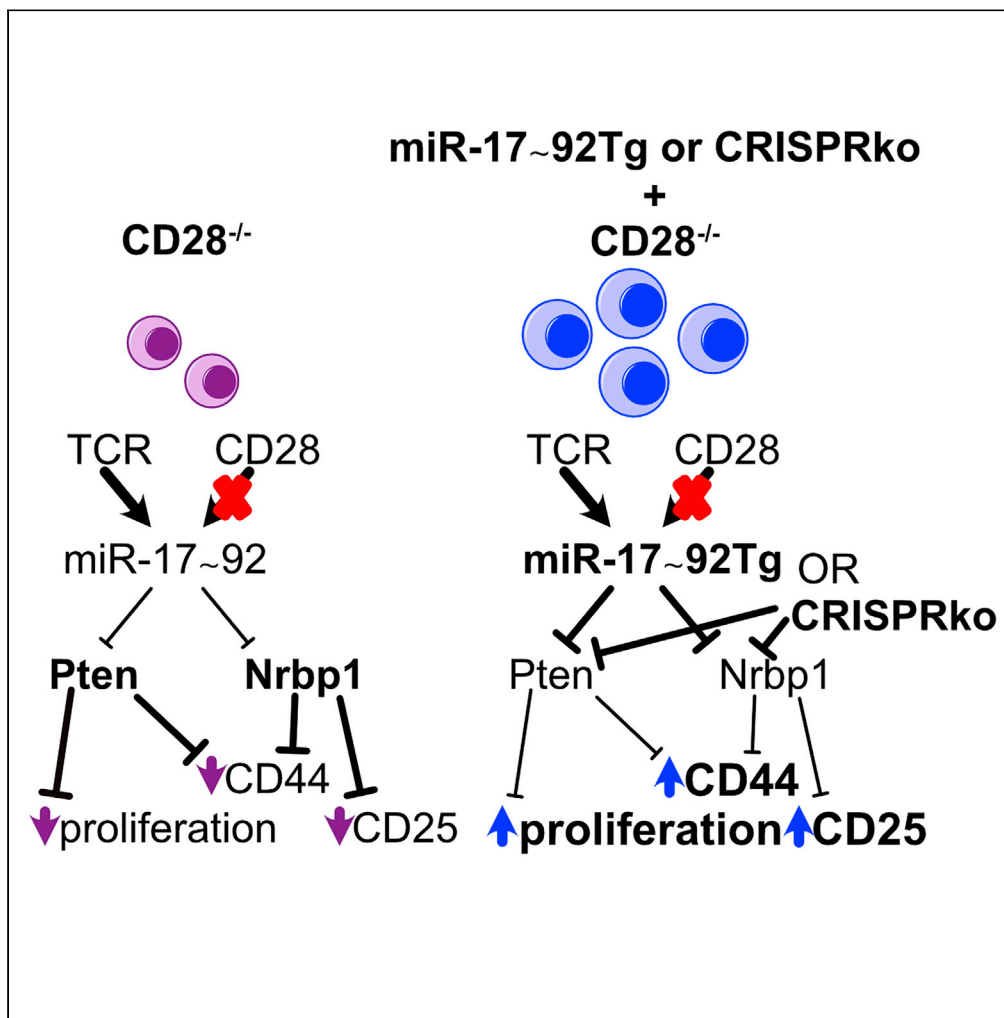


Article

Forced expression of the non-coding RNA miR-17~92 restores activation and function in CD28-deficient CD4⁺ T cells



Marianne Dölz, Marko Hasiuk, John D. Gagnon, ..., Denis Seyres, Julien Roux, Lukas T. Jeker

lukas.jeker@unibas.ch

Highlights

Empirically validated direct miR-17~92 target gene list in mouse CD4⁺ T cells

CD28-deficient CD4⁺ T cells exhibit derepressed miR-17~92 targets during activation

Transgenic miR-17~92 expression rescues CD28-deficiency *in vitro* and *in vivo*

miR-17~92 target KO in naive CD28-deficient CD4⁺ T cells restores distinct phenotypes



Article

Forced expression of the non-coding RNA miR-17~92 restores activation and function in CD28-deficient CD4⁺ T cells

Marianne Dölz,^{1,2} Marko Hasiuk,^{1,2} John D. Gagnon,^{3,4,7} Mara Kornete,^{1,8} Romina Marone,^{1,2} Glenn Bantug,¹ Robin Kageyama,^{3,4} Christoph Hess,^{1,5} K. Mark Ansel,^{3,4} Denis Seyres,^{1,2} Julien Roux,^{1,6} and Lukas T. Jeker^{1,2,9,*}

SUMMARY

CD28 provides the prototypical costimulatory signal required for productive T-cell activation. Known molecular consequences of CD28 costimulation are mostly based on studies of protein signaling molecules. The microRNA cluster miR-17~92 is induced by T cell receptor stimulation and further enhanced by combined CD28 costimulation. We demonstrate that transgenic miR-17~92 cell-intrinsically largely overcomes defects caused by CD28 deficiency. Combining genetics, transcriptomics, bioinformatics, and biochemical miRNA:mRNA interaction maps we empirically validate miR-17~92 target genes that include several negative regulators of T cell activation. CD28-deficient T cells exhibit derepressed miR-17~92 target genes during activation. CRISPR/Cas9-mediated ablation of the miR-17~92 targets *Pten* and *Nrbp1* in naive CD28^{-/-} CD4⁺ T cells differentially increases proliferation and expression of the activation markers CD25 and CD44, respectively. Thus, we propose that miR-17~92 constitutes a central mediator for T cell activation, integrating signals by the TCR and CD28 costimulation by dampening multiple brakes that prevent T cell activation.

INTRODUCTION

T cells are critical to protect mammals from infections and tumors. T cell activation, a key event for adaptive immunity, relies on two signals: T cell receptor (TCR) stimulation as well as costimulation by specialized receptors. While the TCR signal provides specificity, costimulation by antigen-presenting cells (APCs) provides the quantitative and qualitative support for T cell activation (Acuto and Michel, 2003; Esensten et al., 2016). One of the best-studied and prototypical costimulatory molecules is CD28. It promotes multiple processes required for T cell biology such as T cell activation, proliferation, survival, metabolic adaptation, and Interleukin-2 (IL-2) production (Esensten et al., 2016; Riha and Rudd, 2010). These form the basis for clonal expansion and T cell differentiation into a variety of effector T cells that are necessary to mount effective immune responses. Recent data further demonstrates that CD28 expression is not only required for T cell priming but also days later for effector CD4⁺ T cell responses during infection (Linterman et al., 2014).

Due to its centrality for T cell and immune responses more generally, CD28 is an important target in therapeutic immunology (Sansom and Walker, 2013; Esensten et al., 2016; Edner et al., 2020). CD28 blockade by CTLA4-Ig is clinically used to prevent renal allograft rejection and to treat rheumatic disease (Esensten et al., 2016). In contrast, vaccine adjuvants induce the activation of innate immune cells to express ligands that trigger costimulatory molecules on T cells. Furthermore, immune-activating CTLA-4 blocking antibodies represent the foundation of cancer immunotherapy (Leach et al., 1996) and CD28 is required for cancer immunotherapy with PD-1 blocking antibodies (Kamphorst et al., 2017; Hui et al., 2017; Homet Moreno et al., 2016). Finally, CD28 intracellular signaling domains can provide the required costimulatory signal in second and third generation chimeric antigen receptor (CAR) T cell constructs for adoptive cellular therapies (Gross and Eshhar, 2016). Thus, CD28 is a key clinically relevant immunoregulatory receptor and a precise understanding of molecular events induced by CD28 costimulation has direct therapeutic relevance. However, despite intense research, the understanding of the molecular consequences of CD28 costimulation remains incomplete (Esensten et al., 2016; Tian et al., 2015; Liu et al., 2018). CD28 costimulation acts through pleiotropic effects; it promotes the phosphatidylinositol 3-kinase (PI3K) pathway, amplifies the

¹Department of Biomedicine, Basel University Hospital and University of Basel, Hebelstrasse 20, CH-4031 Basel, Switzerland

²Transplantation Immunology & Nephrology, Basel University Hospital, Petersgraben 4, CH-4031 Basel, Switzerland

³Department of Microbiology and Immunology, University of California, San Francisco, San Francisco, CA 94143, USA

⁴Sandler Asthma Basic Research Center, University of California, San Francisco, San Francisco, CA 94143, USA

⁵Department of Medicine – CITIID, University of Cambridge, Puddicombe Way, Cambridge CB2 0AW, UK

⁶Swiss Institute of Bioinformatics, Basel, Switzerland

⁷Present address: ArsenalBio, 571 Eccles Ave, South San Francisco, CA 94080, USA

⁸Present address: Department of Oncology, University of Lausanne, Lausanne, Switzerland, Ludwig Institute for Cancer Research, University of Lausanne, Lausanne, Switzerland

⁹Lead contact

*Correspondence: lukas.jeker@unibas.ch

<https://doi.org/10.1016/j.isci.2022.105372>



TCR signal, stabilizes the transcriptome induced by TCR stimulation, and enhances calcineurin/NFAT signaling (Riha and Rudd, 2010; Esensten et al., 2016; Martinez-Llordella et al., 2013). Collectively, CD28 stimulation ultimately leads to transcriptional changes mediated by the transcription factors (TF) NF- κ B, AP-1, and NFAT (Esensten et al., 2016). In addition, CD28 also acts through many non-transcriptional mechanisms such as mRNA stabilization and altered mRNA splicing (Esensten et al., 2016). Thus, due to the complexity of CD28 costimulation, substantial controversy remains about the importance of various molecular mechanisms and the relative importance of quantitative versus qualitative CD28-mediated signals (Esensten et al., 2016; Acuto and Michel, 2003; Riha and Rudd, 2010; Sansom and Walker, 2013).

Since a protein-centric view prevailed in most studies, here we investigated the role of the microRNA cluster miR-17~92, a non-coding RNA, in CD28 costimulation and T cell activation. MicroRNAs (miRNA) are arguably the best-studied class of non-coding genes. These short RNA molecules of ~22nt length are highly conserved gene repressors that mainly act through base pairing with the 3' untranslated region (UTR) of target RNAs resulting in their decreased abundance and/or translational inhibition (Baumjohann and Ansel, 2013). Together with transcription factors (TFs), miRNAs are the most important *trans*-regulators of gene expression, regulating most mRNAs (Bartel, 2018). Target RNAs can be bound by multiple miRNAs and individual miRNAs can bind to and repress multiple genes, often genes found in the same pathway (Baumjohann and Ansel, 2013). Canonical base-pairing is largely determined by miRNA nucleotide positions 2–7, called the “seed” region (Bartel, 2018) but non-canonical miRNA targeting is widespread and can be equally effective (Loeb et al., 2012; Hsin et al., 2018). The interaction of a miRNA and its target mostly results in mild gene repression, often only reducing protein concentration by less than 2-fold. Nevertheless, miRNA-mediated gene regulation is highly consequential for T cell differentiation and function (Xiao and Rajewsky, 2009; O’Connell et al., 2010; Baumjohann and Ansel, 2013; Jeker and Bluestone, 2013).

We noticed that key functions attributed to CD28 such as T cell proliferation, survival, and T_{FH} differentiation are also regulated by miR-17~92. miR-17~92, a polycistronic transcript induced by CD28 costimulation (de Kouchkovsky et al., 2013), gets processed into 6 mature miRNAs representing 4 different seed families (Xiao and Rajewsky, 2009). Much like CD28, miR-17~92 promotes T cell proliferation, survival, and differentiation (Xiao et al., 2008; Jeker and Bluestone, 2013). Moreover, T cell-specific miR-17~92-deficiency results in severely impaired T_{FH} differentiation and impaired GC formation (Baumjohann et al., 2013; Kang et al., 2013), reminiscent of impaired GC formation observed in CD28-deficient mice (Ferguson et al., 1996). On the contrary, miR-17~92 overexpression results in a systemic lupus-like syndrome with increased GC formation and autoantibody production (Xiao et al., 2008) most likely due to enhanced T_{FH} generation (Kang et al., 2013; Baumjohann et al., 2013).

Here, we show that miR-17~92 was necessary to repress genes in CD28^{-/-} T cells and forced miR-17~92 expression was sufficient to restore an important fraction of the impaired transcriptional regulation and function of CD28-deficiency in murine CD4⁺ T cells. We used transcriptome analysis, computational predictions and biochemical miRNA/target RNA interaction maps to define a high-confidence set of 68 empirically validated direct miR-17~92 target genes in T cells. CRISPR/Cas9-mediated deletion of individual miR-17~92 target genes restored distinct functions in naive CD28^{-/-} T cells. We propose that miR-17~92 acts as an important mediator of T cell activation/CD28-costimulation by repressing multiple inhibitory proteins that restrain T cells from becoming activated.

RESULTS

T cell receptor and CD28 costimulation synergistically induce miR-17~92 expression and forced miR-17~92 expression enables T cell activation of CD28-deficient T cells *in vitro*

miR-17~92 expression has previously been linked to T cell activation/CD28 costimulation (Sandberg et al., 2008; de Kouchkovsky et al., 2013) and the CD28 ligands CD80 and CD86 have a dose-dependent effect on miR-17 expression (Wang et al., 2015). However, the relative contribution of TCR versus CD28 is not well understood. To further investigate this relationship for miR-17~92 induction, we stimulated naive murine CD4 T cells with various combinations of anti-CD3/anti-CD28 monoclonal antibodies (Figure 1A). TCR stimulation alone increased miR-17 expression while isolated CD28 stimulation did not. Compared to low TCR stimulation, high TCR stimulation had a little additional effect on miR-17 but further increased CD69/CD25 expression (Figures 1A and 1B). Adding even a low concentration (0.2 μ g/mL) of anti-CD28 antibody to TCR stimulation increased miR-17 expression at both timepoints (24 and 48 h). The induction of miR-17 progressed from 24 h to 48 h. At any concentration of anti-CD3 mAb stimulation and timepoint, CD28

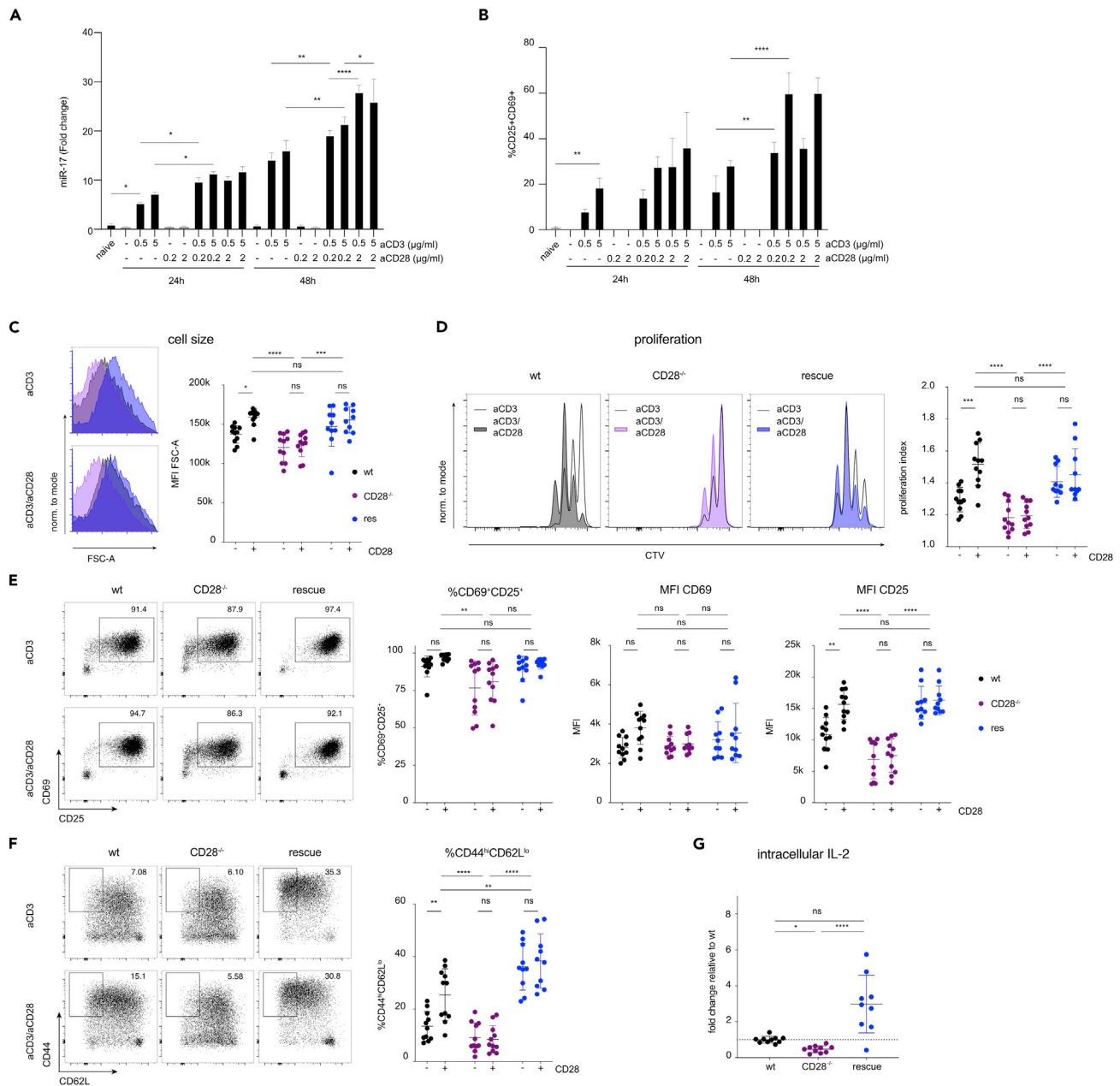


Figure 1. TCR and CD28 costimulation synergistically induce miR-17~92 expression and forced miR-17~92 expression enables T cell activation of CD28-deficient T cells in vitro

(A and B) Naive murine CD4⁺ T cells were activated for 24 h or 48 h using the indicated combinations of plate-bound anti-CD3 and anti-CD28 stimulatory mAbs. (A) miR-17 expression assessed by qPCR. (B) Relative frequencies of cells expressing CD25 and CD69, assessed by flow cytometry. (C–G) wt (black), CD28^{-/-} (purple), rescue (dark blue) CD4⁺ T cells were stimulated for 48 h with plate-bound anti-CD3 with (+) or without (–) anti-CD28. (C) Blasting of CD4⁺ T cells shown as MFI of FSC-A of the lymphocyte gate. (D) Proliferation measured by CTV dilution, gated on viable CD4⁺ T cells. Representative histograms of each genotype activated without (blank) or with (colored) anti-CD28 and quantification of proliferation index. (E and F) Expression of early activation markers CD25/CD69 as well as CD44/CD62L expression. (G) Quantification of flow cytometric intracellular IL-2 staining in CD4⁺ cells stimulated for 3 h with PMA/Iono/BFA. Data from an experiment with 3 biological replicates per condition (A and B). Data from 3 (C–G) independent experiments with 3–4 biological replicates per group. Error bars represent mean ± SD, Tukey's or Hom-Sidak's multiple comparison test; p values: ns = not significant, * < 0.05 ** < 0.002 *** < 0.0002 **** < 0.0001.

costimulation resulted in a positive interaction for miR-17 expression. At both timepoints, the combination of low anti-CD3 (0.5 $\mu\text{g}/\text{mL}$) and low anti-CD28 (0.2 $\mu\text{g}/\text{mL}$) resulted in higher induction of miR-17 than the highest anti-CD3 stimulation alone (5 $\mu\text{g}/\text{mL}$). Finally, at 48 h, low TCR stimulation combined with high CD28 costimulation increased miR-17 but not CD25/69 expression in comparison to low TCR/low CD28 costimulation. In summary, TCR signaling and CD28 costimulation are intricately linked to miR-17 expression (as a surrogate miRNA for the miR-17~92 cluster). Although TCR stimulation alone induced miR-17 expression, combined TCR and CD28 stimulation synergistically increased miR-17 resulting in stronger expression than through either signal alone. These results are consistent with and extend previous experiments using natural ligands that demonstrated a graded control of miR-17~92 by CD28 (Wang et al., 2015).

In order to further investigate the functional connection between CD28 and miR-17~92, we analyzed the consequences of T cell-specific loss and gain of miR-17~92 on key processes regulated by CD28. We compared samples from mice that lack miR-17~92 in T cells (CD4cre.miR-17~92^{lox/lox}, designated T^{1792 Δ/Δ} hereafter), wildtype (wt) mice, and mice overexpressing miR-17~92 in T cells (CD4cre.Rosa26^{lox}STOP^{lox}CAG-miR-17~92Tg, designated T^{1792tg/tg} hereafter). In comparison to wt T cells, proliferation as well as the production and secretion of the CD28-dependent cytokine interleukin-2 (IL-2) was impaired in T^{1792 Δ/Δ} T cells and increased in T^{1792tg/tg} T cells (Figures S1A–S1C) confirming previous findings (Baumjohann et al., 2013; Kang et al., 2013; Steiner et al., 2011). Thus, miR-17~92-deficiency was reminiscent of phenotypes observed in CD28-deficient mice. In contrast, transgenic miR-17~92 had the opposite effect. Thus, the results demonstrated that the non-coding RNA miR-17~92 exerted a dose-dependent regulation of CD4⁺ T cell proliferation and IL-2 production which are known to be CD28-dependent. We hypothesized that miR-17~92 could be a downstream mediator or integrator of T cell activation/CD28 costimulation. To test this hypothesis we crossed B6.CD28^{-/-} (CD28^{-/-}) mice (Shahinian et al., 1993) with T^{1792tg/tg} mice, resulting in B6.CD28^{-/-}.CD4cre.Rosa26^{lox}STOP^{lox}CAG-miR-17~92Tg designated “rescue” hereafter. T cells in these mice lack CD28 but constitutively express transgenic miR-17~92. If miR-17~92 physiologically supported CD28 costimulation then we expected that transgenic miR-17~92 expressions could restore some of the CD28 defects. First, we investigated how “rescue” cells behaved *in vitro*. We compared wt, CD28^{-/-}, and “rescue” naive CD4⁺ T cells stimulated with plate-bound anti-CD3 mAb alone or a combination of anti-CD3 and anti-CD28 mAb. As expected, wt cells blasted (Figure 1C) and increased proliferation (Figure 1D) in response to costimulation compared to anti-CD3 stimulation alone. Compared to wt cells, CD28^{-/-} T cells showed reduced size and proliferation and were unable to respond to anti-CD28 stimulation (Figures 1C and 1D). In contrast, “rescue” T cells stimulated with anti-CD3 alone or combined anti-CD3/anti-CD28 blasted and proliferated like wt T cells fully stimulated with anti-CD3 and anti-CD28 mAb (Figures 1C and 1D).

Next, we turned our attention to surface markers whose expression is either TCR- or CD28-dependent. The early activation marker CD69 is rapidly upregulated during T cell activation and reflects TCR signaling strength (Shang et al., 2018). As a second marker, we used the high affinity IL-2 receptor alpha subunit CD25, a well-known CD28-dependent gene. The relative number of CD69⁺CD25⁺ cells and CD69 expression per cell (Figure 1E) was comparable for all genotypes, as predicted for a TCR-dependent marker. In contrast, the signal intensity of CD25 was clearly CD28-dependent. Wildtype T cells increased CD25 MFI after CD28 costimulation while CD28^{-/-} T cells displayed lower CD25 MFI than wt cells and were unable to respond to CD28 stimulation (Figure 1E). In contrast, CD25 expression was fully restored in “rescue” T cells, even after anti-CD3 stimulation alone (Figure 1E). Finally, CD44 expression was also highly CD28-dependent. In concert with the other CD28-dependent parameters (blasting, proliferation, IL-2, and CD25), wt T cells responded to CD28 ligation with CD44 expression but CD28^{-/-} cells lacked CD44 upregulation. In contrast, the frequency of CD44^{hi}CD62L^{lo} “rescue” T cells was at least comparable to fully costimulated (anti-CD3/anti-CD28) wt T cells (Figure 1F). Thus, the miR-17~92 transgene appeared to efficiently replace CD28 function *in vitro*, restoring the expression of the CD28-dependent markers CD25 and CD44.

Given the remarkable capacity of the miR-17~92 transgene to restore discrete functions in CD28-deficient T cells, we measured miR-17 expression upon activation in various genotypes (Figure S1D). T^{1792 Δ/Δ} T cells were unable to express miR-17 except for a faint signal at 48 h, likely reflecting incomplete deletion. In contrast, wt T cells increased miR-17 at 24 and 48 h while CD28^{-/-} T cells displayed impaired miR-17 expression. Rescue T cells expressed increased miR-17 already in naive T cells and expression further

increased with activation. Expressing one copy of the miR-17~92 transgene in CD28-sufficient T cells increased miR-17 expression compared to wt cells and adding a second transgene copy further increased miR-17 expression. Thus, at 24 h, rescue T cells displayed slightly increased miR-17 expression compared to wt cells and similar expression to wt cells at 48 h. At 48 h, rescue T cells, T^{1792 wt/tg} and T^{1792tg/tg} T cells over-expressed miR-17~92. Overall, these results support the suitability of the chosen experimental system. Finally, since IL-2 production constitutes another functionally important consequence of CD28 costimulation and miR-17~92 correlated strongly with IL-2 production (Figures S1B and S1C), we analyzed this cytokine next. As with blasting or proliferation, CD28-deficient T cells produced less IL-2 but “rescue” T cells produced even supraphysiologic amounts of IL-2 upon activation (Figure 1G). Thus, transgenic miR-17~92 was sufficient to replace CD28 for several costimulation-dependent processes *in vitro*.

Transgenic miR-17~92 enables T cell activation of CD28-deficient T cells *in vivo*

Next, we investigated whether transgenic miR-17~92 could also substitute CD28 function *in vivo*. CD28^{-/-} mice display a severe defect in T_{FH} development and GC formation (Shahinian et al., 1993; Ferguson et al., 1996; Linterman et al., 2009; Walker et al., 1999). Therefore, we infected wt, CD28^{-/-} and “rescue” mice with lymphocytic choriomeningitis virus (LCMV) Armstrong to induce an acute viral infection leading to T_{H1} and T_{FH} differentiation as well as GC B cell formation. Confirming previous literature, we found severely impaired CD44 upregulation, T_{FH} differentiation, and GC B cell formation in CD28^{-/-} mice compared to wt littermates (Figures 2A–2D). In contrast, all these parameters were restored in “rescue” mice (Figures 2A–2D). This is remarkable given the complexity of T_{FH} differentiation (Crotty, 2011). In addition, rescued T cells not only phenotypically resembled T_{FH} cells through their expression of CXCR5, PD-1, Bcl-6, and ICOS (Figures 2B and 2C) but they were functional because they induced GC B cell formation which reflects T_{FH}/B cell crosstalk. Furthermore, the spleen of infected “rescue” mice, but not CD28^{-/-} mice, featured organized GCs containing GL7⁺ B cells and CD4⁺ T cells (Figure 2E) demonstrating the restoration of another hallmark defect found in CD28^{-/-} mice (Ferguson et al., 1996). Finally, we analyzed T_{H1} responses and found that transgenic miR-17~92 restored the defect in T_{H1} differentiation observed in CD28^{-/-} mice (Figures 2F and 2G). We noticed that fewer CD28^{-/-} cells expressed Tbx21 compared to wt cells (Figure 2F). However, some of those cells that did express Tbx21 co-expressed IFN γ , even in CD28^{-/-} cells. Analyzing the ratio of Tbx21⁺IFN γ ⁺/Tbx21⁺ T cells confirmed that the missing costimulatory signal mainly resulted in defective Tbx21 induction rather than IFN γ production (Figure 2H). These results suggest that the CD28^{-/-} defect acts during T cell activation, i.e. before T_{H1} differentiation. Accordingly, the miR-17~92 transgene appears to restore T cell activation signals.

T^{1792tg/tg} T cells displayed increased proliferation and IL-2 secretion compared to wt cells (Figures S1A–S1C) and intracellular IL-2 was not only restored but even higher in “rescue” T cells than wt T cells (Figure 1G), suggesting that the effect of miR-17~92 depended on its abundance. Therefore, we investigated the effect of a single copy of the miR-17~92 transgene in CD28^{-/-} cells. In addition, we directly compared the effect of the miR-17~92 transgene in CD28-deficient and CD28-sufficient T cells *in vivo* to test if CD28 triggering and the miR-17~92 transgene were additive. The effect of various genotypes on miR-17 expression is shown in Figure S1D. We infected CD28^{-/-}, T^{1792 Δ / Δ} , wt, het rescue, rescue, and T^{1792tg/tg} mice with LCMV Armstrong. “het rescue” were CD28^{-/-} that only carried one copy of the miR-17~92 Tg while “rescue” mice were the rescue mice used above (Figures 1 and 2) with two copies of the miR-17~92 transgene. The relative number of CD44⁺ T cells was lowest in CD28^{-/-} and highest in T^{1792tg/tg} mice (Figure S2A). Moreover, CD28^{-/-} and T^{1792 Δ / Δ} mice exhibited similar defects compared to wt mice. In contrast, even one copy of the miR-17~92 Tg was sufficient to rescue the CD28^{-/-} phenotype of T_{FH} and GC B cell formation (Figures S2B–S2D).

In summary, we found an unexpectedly complete the restoration of CD28 costimulatory function and T cell activation exerted by transgenic miR-17~92 expression *in vitro* as well as *in vivo*.

Restoration of T cell activation of CD28-deficient T cells by miR-17~92 is cell intrinsic

Although CD28's main function is on T cells, we sought to formally test whether the miR-17~92-mediated rescue effect was cell intrinsic. We crossed MHC class II-restricted CD4⁺ TCR transgenic mice specific for LCMV (SMARTA; V α 2⁺V β 8.3⁺) to wt, CD28^{-/-} and “rescue” mice. We adoptively transferred (AT) naive CD4⁺ T cells to CD28^{-/-} host mice followed by acute LCMV infection. Eight days post-infection we isolated spleen, mesenteric, and peripheral lymph nodes (LN). In all three organs the frequency and absolute number of V α 2⁺V β 8.3⁺ CD28^{-/-} cells was strongly reduced compared to V α 2⁺V β 8.3⁺ CD28^{wt/wt} cells. In contrast,

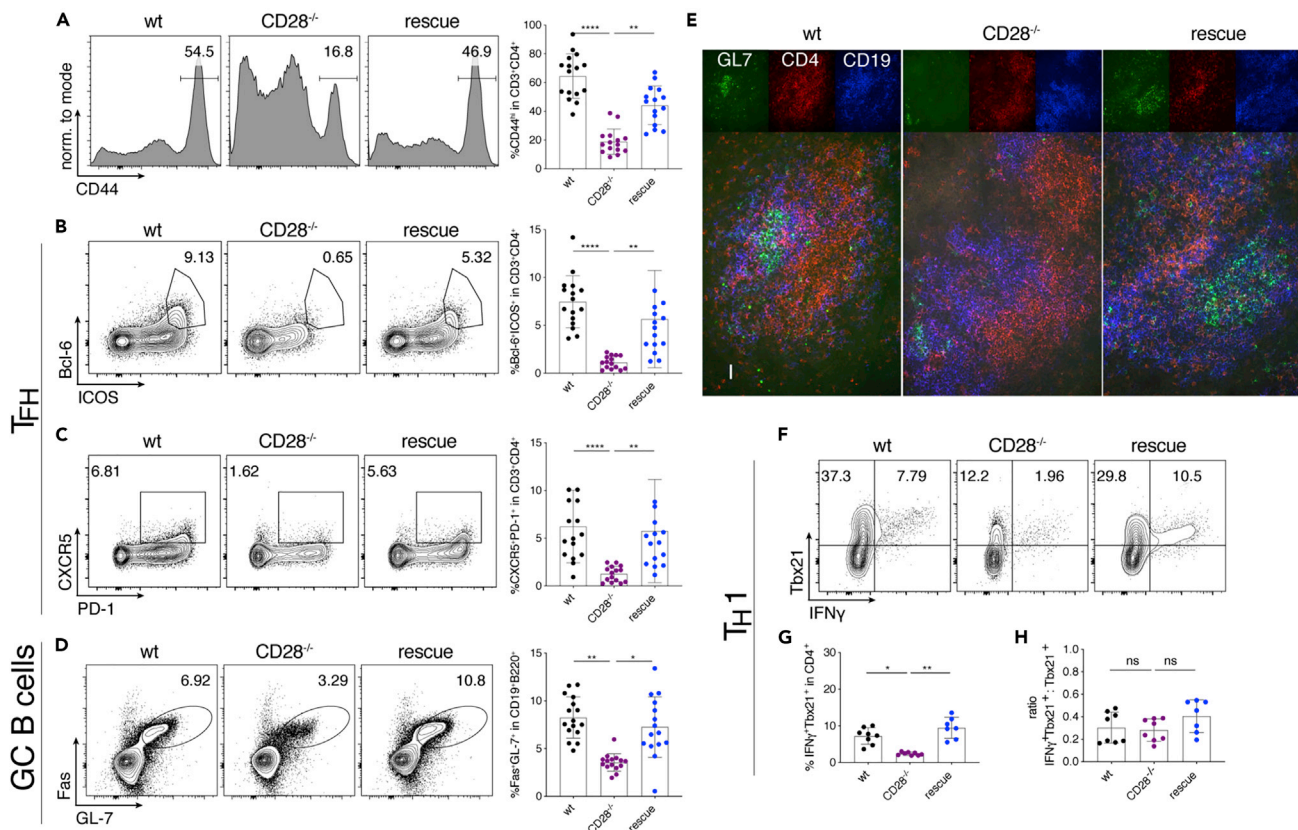


Figure 2. Transgenic miR-17~92 enables T cell activation of CD28-deficient T cells in vivo
6–8 week old mice were infected with LCMV Armstrong; spleens were analyzed at d8 post-infection. wt (black), CD28^{-/-} (purple), rescue (dark blue). (A–D) represent data from 4 independent experiments with 4 mice per group, pre-gating on viable CD4⁺CD3⁺ or viable CD19⁺B220⁺ cells. Representative FACS plots and quantification of relative numbers of (A) CD44 expression, (B) Bcl6⁺ICOS⁺ population (T_{FH}), (C) CXCR5⁺PD-1⁺ population (T_{FH}) and (D) Fas⁺GL7⁺ population (GC B cells). (E) Cryosections of spleens stained for GL-7 (green), CD4 (red) and CD19 (blue). Scale bar 40 μ m. (F–H) Splenocytes were re-stimulated with GP-64 and BFA for 4 h and investigated for T_{H1} phenotype, pre-gated on viable CD3⁺CD4⁺ cells. Shown are 3 independent experiments with 4 biological replicates per group. Representative FACS plots (F) and quantification (G) of relative numbers of Tbx21⁺IFN γ ⁺ CD3⁺CD4⁺ cells. (H) Ratio of Tbx21⁺IFN γ ⁺ to total Tbx21⁺ cells. Error bars represent mean with SD, Dunn's multiple comparison test; p values: ns = not significant, *<0.05, **<0.002, ***<0.0002, ****<0.0001.

the miR-17~92 transgene restored relative and absolute numbers of $V\alpha 2^+V\beta 8.3^+$ CD28^{-/-} T cells (Figures 3A, S3A, and S3B). Furthermore, among $V\alpha 2^+V\beta 8.3^+$ T cells, fewer CD28^{-/-} cells upregulated CD44 than in wt cells, a defect that was entirely restored in rescue cells (Figures 3B, S3C, and S3D). Thus, these data unequivocally demonstrate that transgenic miR-17~92 cell intrinsically compensated for CD28 deficiency.

miR-17~92 shapes the transcriptome after CD4⁺ T cell activation

To unravel the molecular mechanism underlying miR-17~92-mediated function during T cell activation we performed RNA-sequencing on naive and *in vitro* activated (24 and 48 h) CD4⁺ T cells from T^{1792 Δ / Δ} , wt, and T^{1792tg/tg} mice. Principal component analysis (PCA) revealed that the transcriptomes of naive T cells from all three genotypes were very similar (Figure 4A, 0 h). T cell activation induced major changes in gene expression (PC1, 56.7% of variance explained and PC2, 14% of variance explained) and also made the genotypes separate at 24 h and even more clearly at 48 h after activation (Figures 4A and S4A) (PC1 and PC3, 7.2% of variance explained). Since miRNAs often repress individual genes only mildly (Bartel, 2018), we compared the most extreme genotypes, i.e. T^{1792 Δ / Δ} to T^{1792tg/tg} to increase the power of differential gene expression analysis, at each time point. At a false discovery rate (FDR) of 1%, the number of differentially expressed genes (DEG) increased over time (830 genes up-regulated and 789 genes down-regulated at 0 h, 2,493 up and 2,370 down at 24 h, and 3,173 up and 3,242 down at 48 h). Unsupervised hierarchical clustering

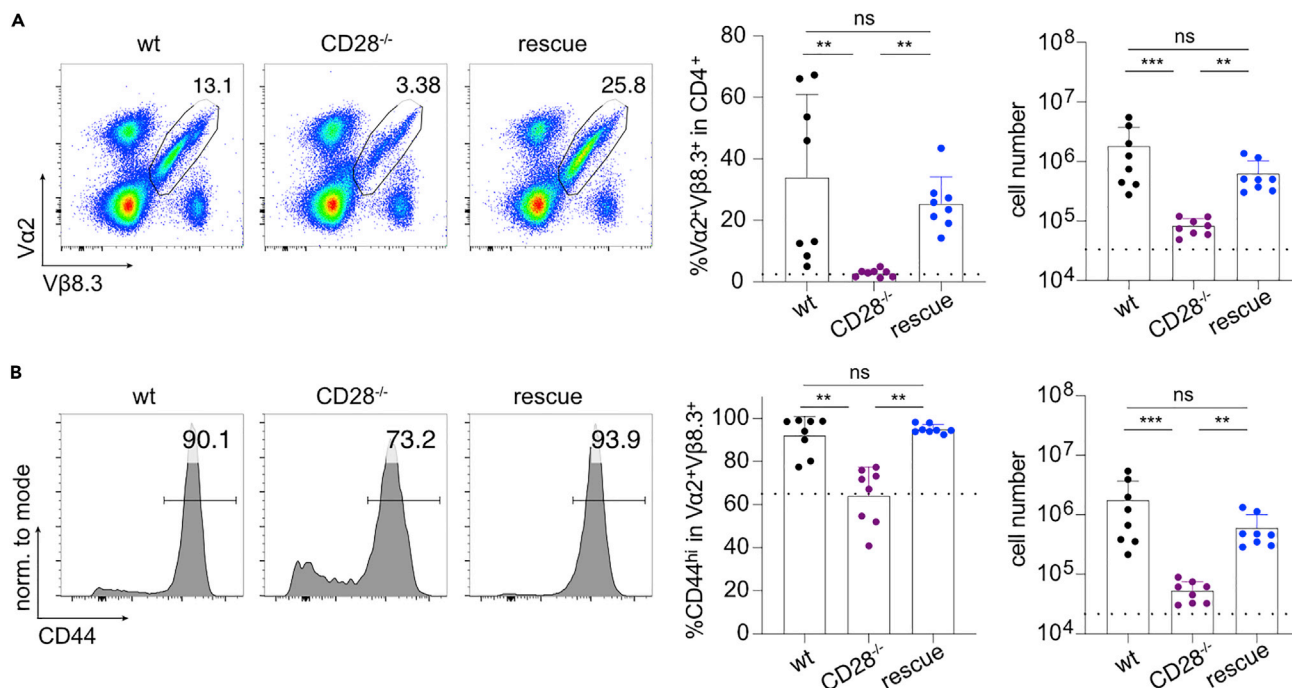


Figure 3. Restoration of T cell activation of CD28-deficient T cells by miR-17~92 is cell intrinsic

Adoptive transfer of naive SMARTA⁺ CD4⁺ T cells into CD28^{-/-} hosts, subsequent LCMV Armstrong infection, and analysis of organs at d8 post-infection. Donor genotypes wt (black), CD28^{-/-} (purple), rescue (dark blue). Dotted line indicates recipient's intrinsic Vα2⁺Vβ8.3⁺ population measured in a non-transferred control host.

(A and B) (A) Vα2⁺Vβ8.3⁺ cells from peripheral LN pre-gated on viable, CD3⁺CD4⁺ cells (B) CD44 expression in Vα2⁺Vβ8.3⁺ population from peripheral LN. 2 independent experiments, 4 recipients per group. Error bars represent mean ± SD, Dunn's multiple comparison test, p values: ns = not significant, * < 0.05, ** < 0.002, *** < 0.0002. See also Figure S3 for spleen and mesenteric LN.

of DEG 24 h after activation revealed a nuanced pattern of gene clusters (Figure 4B). As expected from the PCA (Figure 4A), gene expression across genotypes was very similar in naive T cells and the magnitude of expression differences increased after activation (Figure 4B). According to their expression profile, we highlighted 4 different groups of genes (Figure 4B): cluster I genes were induced over time and enhanced in T^{1792tg/tg} compared to wt but reduced or delayed in T^{1792Δ/Δ}. Cluster II genes decreased with time and miR-17~92 supported their repression. Overall cluster III gene expression increased after activation but expression per time point inversely correlated with the genotype (T^{1792Δ/Δ} > T^{1792tg/tg}). Thus, miR-17~92 limited the maximal expression of genes in this group after induction. Finally, genes displaying the most obvious inverse correlation with the genotype were grouped in clusters IVa and IVb.

To disentangle the gene regulation modalities of the different clusters, we used exon-intron split analysis (EISA) to discriminate between transcriptional versus posttranscriptional regulation (Gaidatzis et al., 2015a). In addition, we employed computational target gene predictions for miR-17~92 from the Targets-can ("TS") database (Agarwal et al., 2015) and used a dataset of biochemically detected direct miRNA:mRNA interactions in T cells defined by Argonaute 2 high-throughput sequencing of RNA isolated by crosslinking immunoprecipitation ("AHC") (Gagnon et al., 2019). For each gene, we quantified the read coverage on TS seed matches for each of the miR-17~92 cluster seed families. These predictors of transcriptional ("DE intron," for differential expression pattern detected at the nascent transcripts) and post-transcriptional regulation ("TS," "AHC"), annotated on the heatmap (Figure 4B) revealed different patterns of regulation for the 4 groups of genes highlighted above. Cluster I genes were enriched for transcriptional regulation (both DE and DE intron) and displayed few TS sites or AHC reads (Figure 4B, box I). Thus, they were mainly induced by increased gene transcription, and miR-17~92 promoted this transcriptional activity. Examples include *Cd44*, *IL-21*, *Tbx21*, and *IFNγ* (Figure 4C). In contrast, genes from clusters IVa and IVb (Figure 4B, boxes IVa, IVb), which displayed a colinear reduction of expression levels across genotypes, contained few transcriptionally regulated genes but were enriched for TS sites (p value = 0.001037; Fisher test) and experimentally determined AHC reads (p value = 0.003598; Fisher

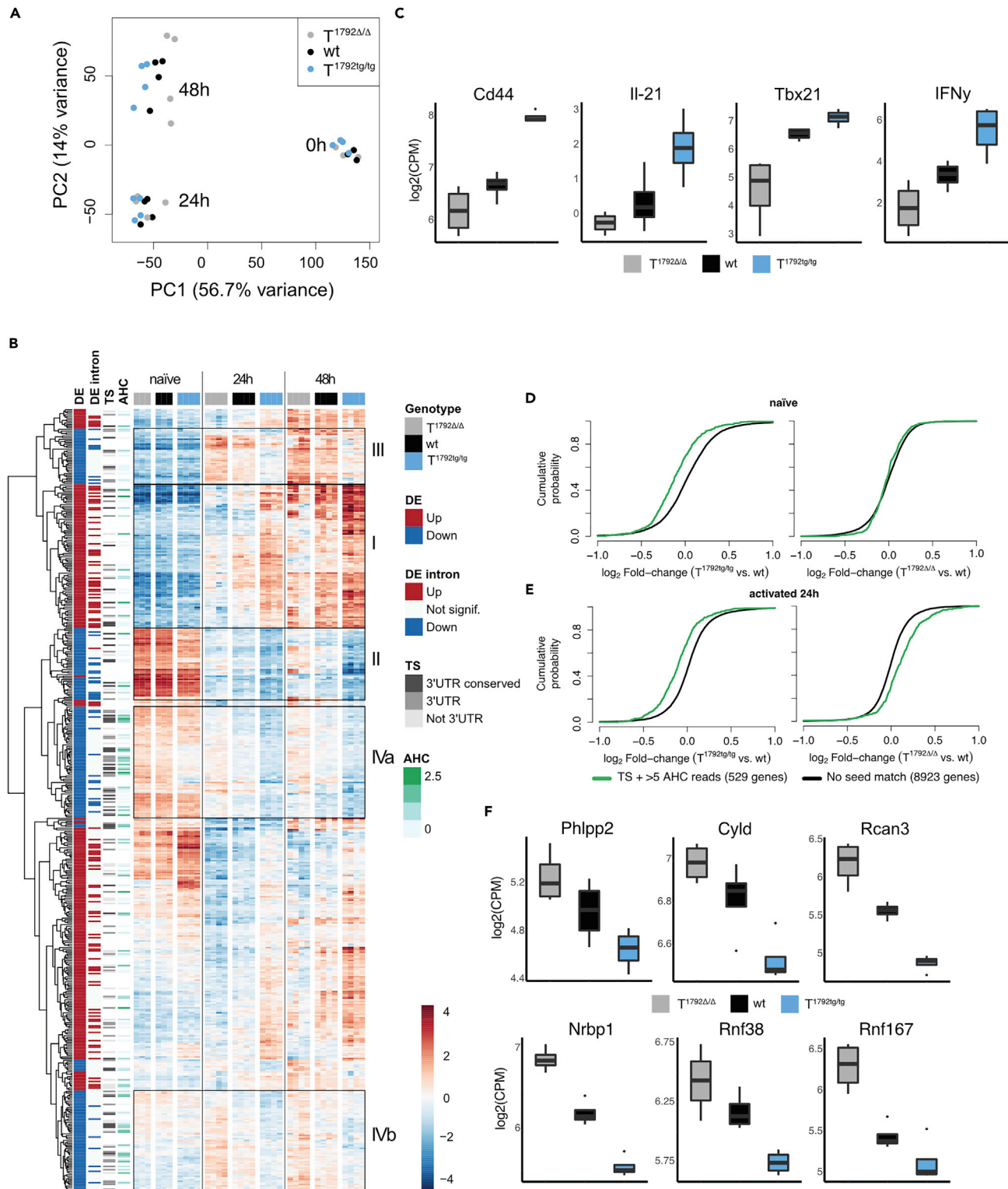


Figure 4. miR-17~92 shapes the transcriptome after CD4⁺ T cell activation

Naive CD4⁺ T cells from $T^{1792\Delta/\Delta}$ (gray), wt (black) and $T^{1792tg/tg}$ (light blue) were activated with plate-bound anti-CD28 and anti-CD3 for 0, 24, and 48 h. Total RNA was extracted for bulk RNA sequencing.

(A) PCA (PC1 vs. PC2) based on the 25% most variable genes.

Figure 4. Continued

(B) Hierarchical clustering of the set of genes selected with $\text{abs}(\log_2\text{FC}) > 1$ & $\text{adj.P.Val} < 0.001$ in the $T^{1792\text{tg/tg}}$ vs. $T^{1792\Delta/\Delta}$ comparison at 24 h. The heatmap displays the centered log of counts per million, with blue indicating low and red indicating high expression. Annotations: “DE” indicates the fold change direction, “DE intron” indicates if significant changes are observed in EISA analysis, “TS” indicates presence (gray) or absence (blank) of a seed match and its location and “AHC” indicates the 3’UTR signal intensity in HITS-CLIP data. Boxes I–IVb designate gene clusters.

(C) Examples of genes in cluster I.

(D and E) Genome-wide transcriptome analysis presented as the \log_2 value of the gene-expression ratio for each gene versus the cumulative fraction of all \log_2 ratios in naive (D) and 24 h activated (E). Shown is the miR-17 seed family for $T^{1792\text{tg/tg}}$ vs. wt and $T^{1792\Delta/\Delta}$ vs. wt comparisons. Black curve: all genes without a seed match and ≤ 5 AHC reads; green: subset of genes with a seed sequence for the seed family and > 5 reads in the AHC.

(F) Examples of genes defined as empirically validated miR-17~92 targets. \log_2 RNA expression level in activated CD4^+ T cells, numbers correspond to $\text{FDR} < 0.05$. Boxplot representing values distribution over minimum and maximum values, median, 25th and 75th percentiles.

test) (Figure 4B). Thus, these clusters were mainly regulated posttranscriptionally and were likely enriched for direct miR-17~92 target genes.

To further characterize direct miR-17~92 target genes we focused on naive T cells and the 24 h time point since indirect effects likely increased after this time point. To visualize the effect of individual miR-17~92 cluster miRNAs on their target genes we compared the expression of genes identified by TS and with > 5 AHC reads for each miRNA seed family to all genes without any seed match for that family. As illustrated by the miR-17 seed family, the miR-17~92 transgene repressed miR-17 target genes in naive T cells (Figure 4D, left panel) but the absence of miR-17~92 had no effect on the expression of miR-17 target genes (Figure 4D, right panel). In contrast, after T cell activation miR-17 target genes were repressed in $T^{1792\text{tg/tg}}$ T cells (Figure 4E, left panel) and derepressed in $T^{1792\Delta/\Delta}$ T cells (Figure 4E, right panel). Similar effects were observed for all seed families although to a lesser extent for the miR-18 seed family (Figures 4B and 4C). We defined genes as empirically validated miR-17~92 targets if they fulfilled the following criteria: i) significant derepression in $T^{1792\Delta/\Delta}$ vs wt and significant repression in $T^{1792\text{tg/tg}}$ vs wt at 24 h ii) predicted TS match iii) > 5 AHC reads and iv) posttranscriptional regulation based on EISA. Applying these criteria across the 4 seed families from miR-17~92 defined a set of 68 empirically supported direct miR-17~92 target genes (Table S1). These genes included previously described miR-17~92 targets validated in T cells, such as *Phlpp2* (Kang et al., 2013) and *Cyld*, validated in B cells (Jin et al., 2013) (Figure 4F). In addition, this approach identified many less studied genes (e.g. *Rcan3*, *Nrbp1*, *Rnf38*, and *Rnf167*) (Figure 4F). Notably, several of the target genes negatively regulate pathways important for T cell activation. For instance, *Phlpp2* is a PI3K inhibitor (Kang et al., 2013) and *Cyld* is an NF- κ B inhibitor (Reiley et al., 2007). In addition, we identified the putative calcineurin inhibitor *Rcan3* (Mulero et al., 2007) as a new miR-17~92 target and validated its RNA-Seq data by qPCR on independent biologic replicates (Figure S4D). Its 3’UTR contains a conserved miR-17-5p 8mer binding site and AHC confirmed a single discrete peak at this site, evidence for a direct interaction of a miRNA with the *Rcan3* 3’UTR in primary T cells (Figure S4E and (Loeb et al., 2012; Gagnon et al., 2019)). Together, these data empirically validate *Rcan3* as a miR-17 target in T cells.

Thus, using a combination of experimentally validated differential gene expression ($T^{1792\Delta/\Delta}$, wt, and $T^{1792\text{tg/tg}}$ T cells), evidence of posttranscriptional gene regulation and biochemical detection of miRNA binding we defined a high confidence set of miR-17~92 target genes in T cells. miR-17~92 became functionally relevant after T cell activation and shaped the transcriptome in intricate ways. Our data demonstrate that miR-17~92 can promote and inhibit gene expression, through posttranscriptional gene regulation, enhancing gene silencing or dampening expression of induced genes. Thus, miR-17~92-mediated gene repression is important to shape the T cell transcriptome during T cell activation.

miR-17~92 promotes the calcineurin/NFAT pathway in CD4^+ T cells

To identify which molecular pathways were regulated by miR-17~92, we analyzed curated gene sets enriched for differentially expressed genes between $T^{1792\text{tg/tg}}$ and $T^{1792\Delta/\Delta}$. At 24 h, the gene sets with the highest statistical significance and largest average fold change were related to cytokines, inflammation, and T cell differentiation (Figure S5A) while at 48 h many metabolic pathways were altered (Figure S5B). Next, we performed enrichment analysis on DoRothEA regulons (Garcia-Alonso et al., 2019) to identify TF activity that could explain the regulated pathways. Regulons were defined using any existing documented interaction with a particular TF. At 24 h, the five most significantly enriched TF regulons with the highest fold change contained two NFAT members (NFATC2, NFATC3) as well as RELA, NF- κ B1, and GATA3 (Figure 5A). Since NFAT TFs are important for T cell activation and differentiation (including T_{FH} differentiation (Martinez et al., 2016)) but miR-17~92 is not known to promote NFAT activity in

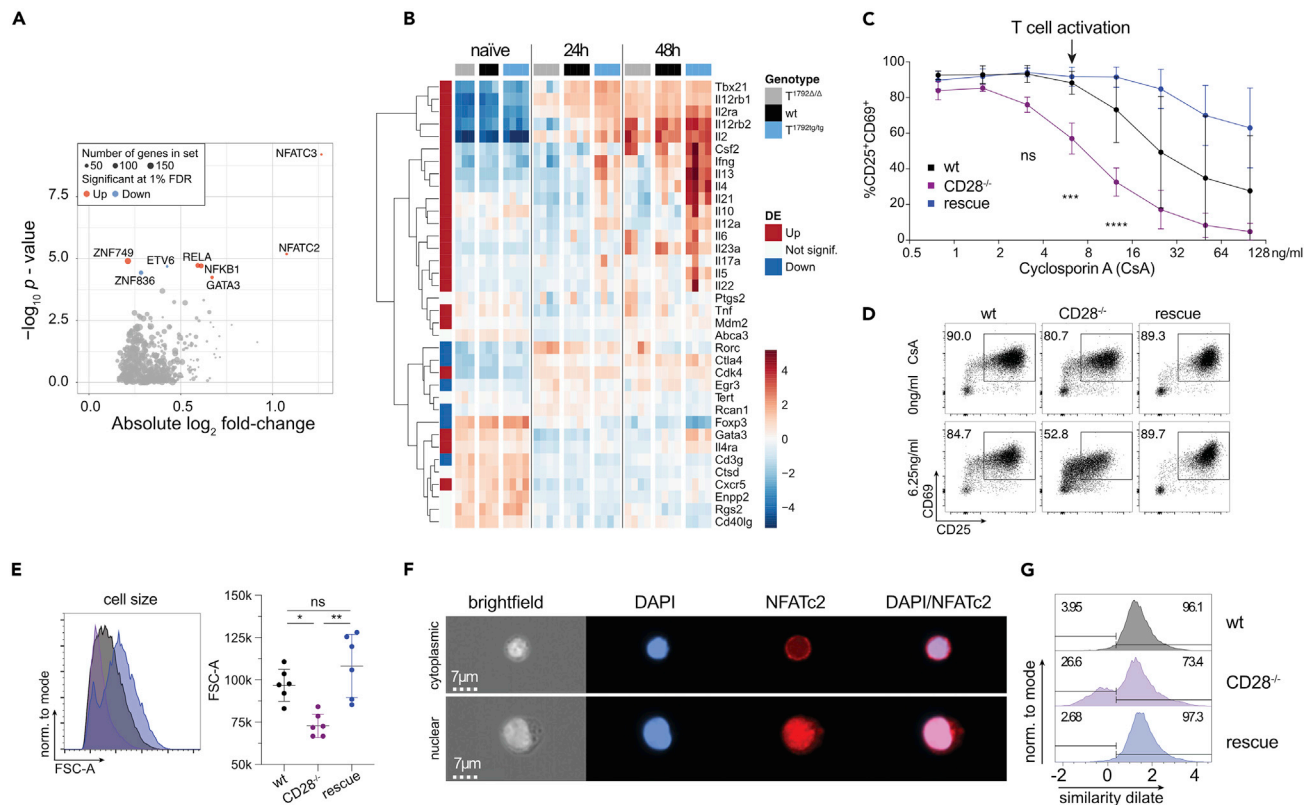


Figure 5. miR-17~92 promotes the NFAT and NF- κ B pathways in CD4⁺ T cells

(A and B) Dataset from Figure 4. Naive CD4⁺ T cells from $T^{1792\Delta/\Delta}$ (gray), wt (black), and $T^{1792tg/tg}$ (light blue) were activated with plate-bound anti-CD28 and anti-CD3 for 0, 24, and 48 h. Total RNA was extracted for bulk RNA sequencing. (A) Volcano plot showing the absolute \log_2 fold change and $-\log_{10}$ p value from regulon analysis. A threshold of 1% FDR was applied. Dot size indicates the number of genes within each regulon and colors indicate fold change direction. (B) Heatmap of genes under NFATC2_D and NFATC3_D regulons plus several known activated genes in CD4⁺ T cells (Il10, Il12a, Il6, Rorc, Il23a). Hierarchical clustering was applied on genes. Centered log of counts per million is displayed, with blue indicating low and red indicating high expression. (C) CD4⁺ wt (black), CD28^{-/-} (purple), and rescue (dark blue) cells were activated for 48 h in the presence of increasing concentrations of cyclosporin A (CsA) as indicated and stained for CD25 and CD69. Shown are 2 independent experiments, error bars represent means \pm SD. Tukey's multiple comparison, p values: ** < 0.002, **** < 0.0001 refer to the difference between CD28^{-/-} and wt.

(D) representative FACS plots of CD25/CD69 expression in viable CD4⁺ T cells activated for 48 h with no or 6.25 ng/ml CsA.

(E) influence of 6.25 ng/ml CsA on blasting (FSC-A of the lymphocyte gate) of viable CD4⁺ cells.

(F) Imagestream analysis of CD4⁺ T cells, activated for 48 h in presence of 6.25 ng/ml CsA; DAPI (blue) and NFATc2 (red) staining. Examples for cytoplasmic (top) and nuclear (bottom) NFATc2 in a CD28^{-/-} sample.

(G) histograms of the similarity dilate indicative of the co-localization of NFATc2 and DAPI signals; gates indicate the nuclear (high similarity dilate) and the cytoplasmic population (low similarity dilate).

See also Figures S5 and S6.

T cells, we focused on the calcineurin/NFAT axis. Genes belonging to regulons NFATC2 and NFATC3 include many T cell lineage-defining TFs, cytokines, and cytokine receptors and most of them – including *IL-21*, *Tbx21*, and *IFN γ* (Figure 4C) – were regulated by miR-17~92 (Figure 5B). This confirmed that miR-17~92 constitutes a central regulator of T cell activation and suggested that transgenic miR-17~92 enhanced canonical pathways that resulted in the functional substitution of CD28 for the differentiation of T_{FH} and T_{H1} *in vivo* (Figure 2). Since miR-17~92 promoted the expression of signature TF and cytokines defining multiple T cell subsets, we tested if miR-17~92 more generally could replace CD28. To this end, we differentiated T_{H1} , T_{H17} , and *iTreg* cells *in vitro*. We confirmed that also in this setup transgenic miR-17~92 was sufficient to compensate for the absence of CD28 and functionally corrected the defects of CD28^{-/-} T cells to differentiate into all 3 subsets (Figure S6).

While miR-17~92 predominantly promoted inflammatory pathways at 24 h, at 48 h several metabolic pathways were regulated by miR-17~92 (Figures S5A and S5B). Thus, we hypothesized that initial transcriptional

changes could lead to altered metabolism. It was recently shown that cell cycle entry of quiescent T cells was controlled by store-operated Ca^{2+} entry (SOCE) and calcineurin/NFAT through control of glycolysis and oxidative phosphorylation (Vaeth et al., 2017). Therefore, we analyzed T cell metabolism in naive and activated $\text{T}^{1792\Delta/\Delta}$, wt, and $\text{T}^{1792\text{tg}/\text{tg}}$ T cells. In line with the transcriptome results (Figure 4), metabolic flux analysis demonstrated comparable glycolytic and respiratory activity of naive T cells in $\text{T}^{1792\Delta/\Delta}$, wt, and $\text{T}^{1792\text{tg}/\text{tg}}$ T cells (Figures S5C and S5D). In contrast, 48 h after activation, glycolytic and respiratory activity positively correlated with the miR-17~92 genotype (Figure S5E and S5F). Furthermore, genes associated with the TCA cycle and respiratory electron transport positively correlated with miR-17~92 at 48 h but not before, supporting the notion that miR-17~92 indirectly promoted this metabolic activity (Figure S5G).

Since transcriptome analysis identified NFAT as a key pathway promoted by miR-17~92 (Figures 5A and 5B), we designed experiments to functionally validate this increased activity. We activated wt, $\text{CD28}^{-/-}$ and “rescue” T cells in the presence of cyclosporin A (CsA), a drug known to inhibit calcineurin/NFAT, and quantified CD69/CD25 expression. Compared to wt cells, $\text{CD28}^{-/-}$ cells were 4-fold more sensitive to CsA (Figure 5C). At a CsA concentration that did not affect wt cells (arrow in Figure 5C), T cell activation of $\text{CD28}^{-/-}$ T cells was clearly inhibited (Figures 5C and 5D). Thus, compared to wt cells $\text{CD28}^{-/-}$ T cells are hypersensitive to CsA. In contrast, $\text{CD28}^{-/-}$ T cells with forced miR-17~92 expression (rescue cells) were normally activated (Figures 5C and 5D). In fact, at higher CsA concentrations the “rescue” T cells were even more resistant to CsA inhibition than wt T cells (Figure 5C). These findings were further corroborated by the analysis of cell size which revealed that in the presence of low dose CsA the blasting defect of $\text{CD28}^{-/-}$ T cells was compensated for by transgenic miR-17~92 (Figure 5E). Finally, we assessed the nuclear translocation of activated NFATC2 as a direct readout of calcineurin activity. ImageStream analysis of T cells activated in the presence of 6.25 ng/mL CsA showed T cells with cytoplasmic (top row) or nuclear (lower row) NFATC2 (Figure 5F). Quantification of this data demonstrated that the presence of a low CsA concentration reduced nuclear NFATC2 translocation in $\text{CD28}^{-/-}$ T cells but was restored in “rescue” cells (Figure 5G). Thus, the miR-17~92 transgene replaced CD28 -enhanced NFAT signals for blasting, CD69/CD25 upregulation, and nuclear translocation of NFATC2.

miR-17~92 is necessary for the repression of a subset of genes during T cell activation

Next, we examined whether miR-17~92 was physiologically required to shape the molecular program triggered by CD28 engagement. We repeated transcriptome analysis with RNA-seq on naive and activated (24 h) CD4^+ T cells from $\text{T}^{1792\Delta/\Delta}$, wt, and $\text{T}^{1792\text{tg}/\text{tg}}$ mice but added $\text{CD28}^{-/-}$ and “rescue” T cells. The correlation of miR-17~92 target gene expression levels with the first RNA-seq experiment (Figure 4) was very high (Figure S7A). A PCA showed that the transcriptomes of naive T cells of all 5 genotypes were closely related (Figure 6A). However, after T cell activation (PC1, 67.6% of variance) the 5 genotypes formed 5 distinct groups that were separated on PC2 (5.6% of variance). Notably, the “rescue” samples were located between $\text{CD28}^{-/-}$ and $\text{T}^{1792\Delta/\Delta}$, wt, and $\text{T}^{1792\text{tg}/\text{tg}}$ T cells (Figure 6A). This implied that transgenic miR-17~92 partially restored the genetic networks dysregulated by CD28 deficiency, supporting the notion that the phenotypic rescue (Figures 1–3) was not a transgene artifact. Moreover, compared to all genes without a miR-17 seed match, the miR-17 target gene set based on the same criteria specified earlier but using a second dataset differential gene expression analysis was overall derepressed in $\text{CD28}^{-/-}$ T cells compared to wt cells (Figures 6B and S7B). It is important to note that these cells have an untouched miR-17~92 locus and therefore should repress miR-17~92 target genes similar to wt cells. However, the absence of CD28 resulted in increased expression of those genes. This result demonstrated that CD28 -dependent effects normally rely on miR-17~92 to repress dozens of genes during T cell activation. Remarkably, the expression of target genes was corrected in “rescue” cells (Figures 6C and S7B). Thus, transgenic miR-17~92 repressed the physiologic targets that were derepressed in $\text{CD28}^{-/-}$ T cells.

However, the molecular rescue effect on the entire transcriptome was incomplete (Figure 6A). We, therefore, analyzed which transcripts were restored and whether they were regulated transcriptionally or post-transcriptionally. Similarly to Figure 4B, we selected genes differentially expressed in the $\text{T}^{1792\Delta/\Delta}$ to $\text{T}^{1792\text{tg}/\text{tg}}$ comparison at 24 h, and performed unsupervised hierarchical clustering using their gene expression profiles across all 5 genotypes. At 24 h, one gene cluster stood out in which “rescue” T cells were more similar to wt and $\text{T}^{1792\text{tg}/\text{tg}}$ cells than $\text{CD28}^{-/-}$ and $\text{T}^{1792\Delta/\Delta}$ cells (Figure 6D, box). Genes in this cluster contained several NFAT-dependent transcripts including *IL-4*, *IL-12a*, *IL12rb2*, *IL-21* and *IFN γ* (Table S2, Figure 5B). Importantly, *Cd44*, *IL-21*, *Tbx-21*, and *IFN γ* transcripts, also contained in this cluster, were reduced in $\text{CD28}^{-/-}$ compared to wt cells (Figure 6E). In contrast, transgenic miR-17~92 partially or completely

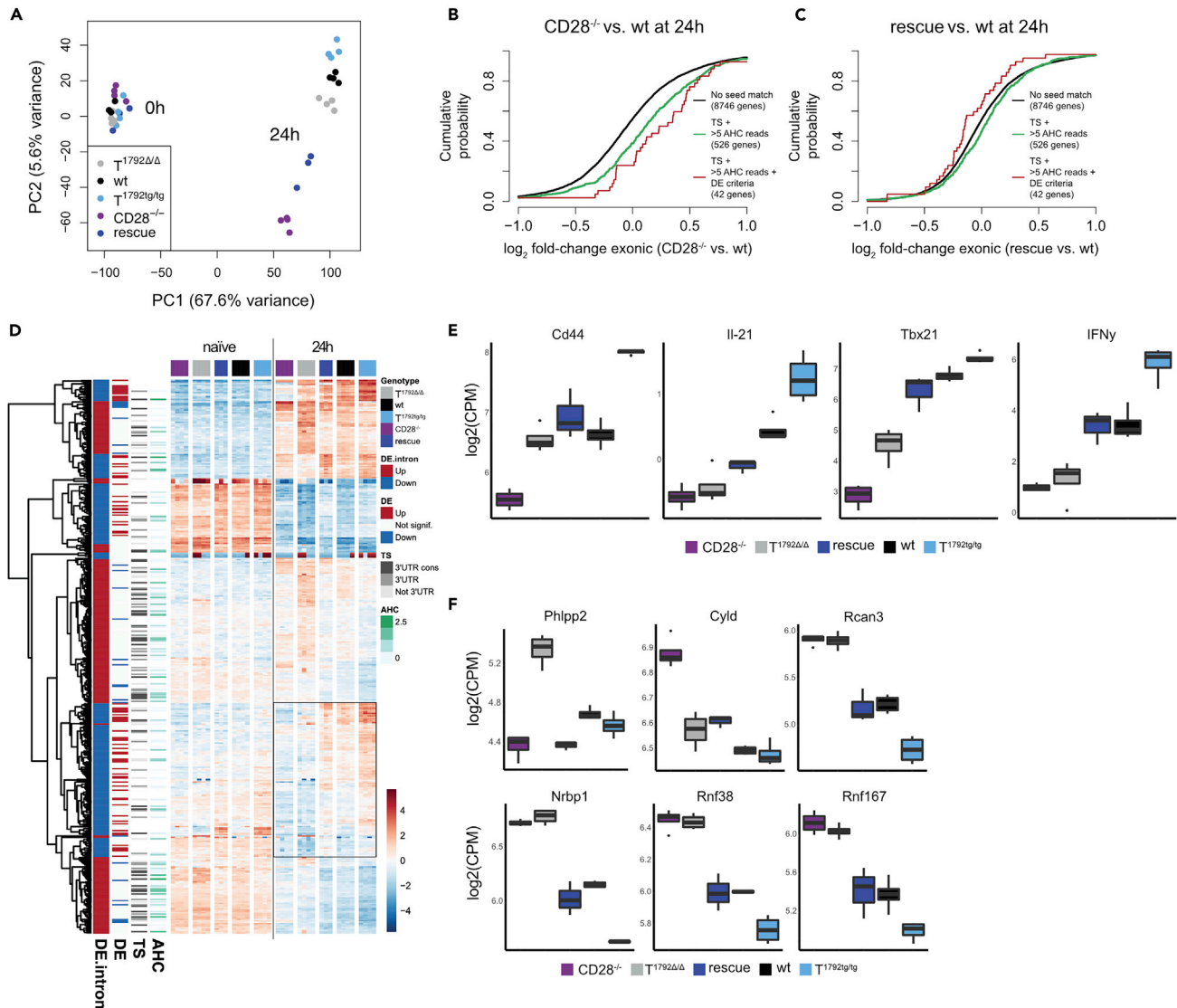


Figure 6. miR-17~92 is necessary for repression of a subset of genes during T cell activation

CD4⁺ T cells from T^{1792Δ/Δ} (gray), wt (black), T^{1792tg/tg} (light blue), CD28^{-/-} (purple) and rescue (dark blue) mice were activated for 24 h. Total RNA was extracted for sequencing.

(A) PCA (PC1 vs. PC2) based on the 25% most variable genes.

(B and C) (B) Genome-wide transcriptome analysis, presented as the log₂ value of the gene-expression ratio for each gene versus the cumulative fraction of all log₂ ratios. Shown are the contrasts between activated samples separated by the miR-17 seed family for the comparison CD28^{-/-} vs. wt (B) and rescue vs. wt (C). Black curve: genes without a seed match, ≤5 AHC reads, and no differential expression in the second RNA sequencing. Green: genes with a conserved binding site for the miR-17 seed family (TS) and >5 reads in the AHC, red: genes with a conserved binding site for the miR-17 seed family (TS), >5 reads in the AHC and differential expression in the second RNA sequencing dataset.

(D) Hierarchical clustering of the set of genes selected with abs(log₂FC) > 1 & adj.P.Val < 0.001 in the T^{1792tg/tg} vs. T^{1792Δ/Δ} comparison at 24 h. The heatmap displays the centered log of counts per million, with blue indicating low and red indicating high expression.

(E) Examples of transcripts that were restored in “rescue” compared to CD28^{-/-} T cells, i.e. contained in the box (D).

(F) Examples of direct miR-17~92 targets. E, F: log₂ mRNA expression (counts per million) in activated CD4⁺ T cells; numbers correspond to FDR < 0.05. Boxplot representing values distribution over minimum and maximum values, median, 25th and 75th percentiles.

See also Figure S7.

restored these transcripts in “rescue” cells to wt levels. Furthermore, T^{1792tg/tg} T cells expressed supraphysiologic mRNA levels (Figure 6E). Thus, the phenotypic rescue of CD44 and IFN γ in CD28^{-/-} T cells (Figures 1–3) could at least partially be attributed to increased expression of these genes driven by the miR-17~92 transgene in “rescue” cells.

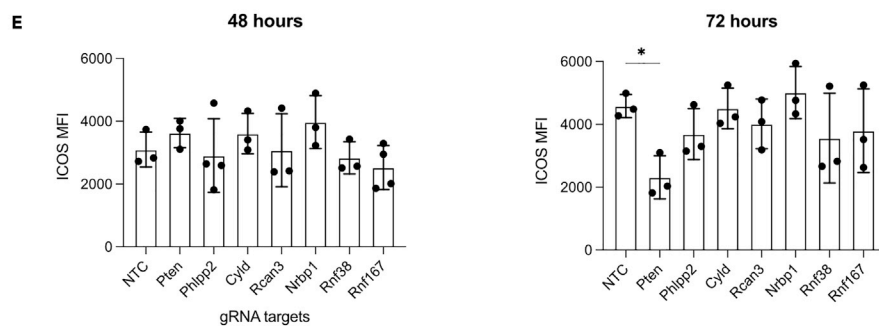
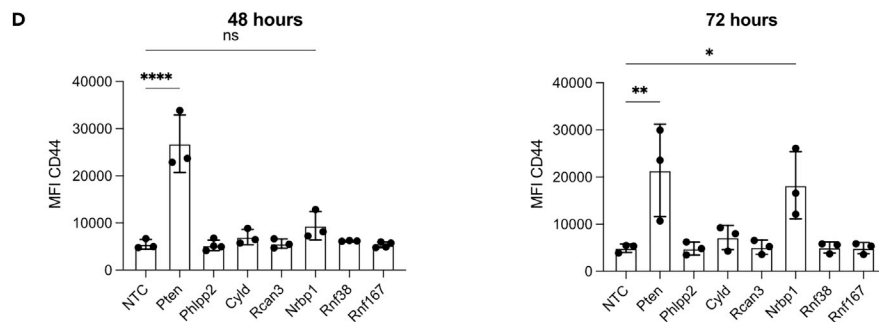
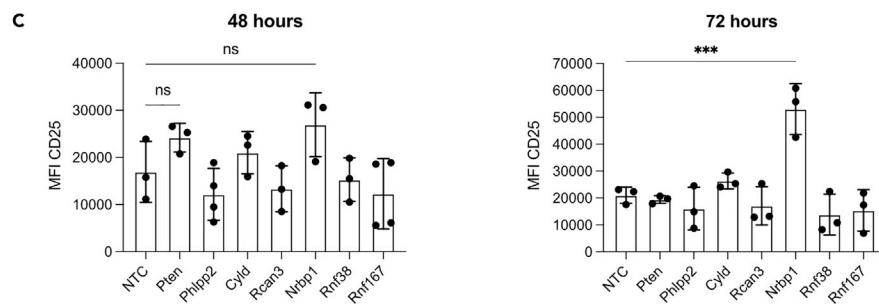
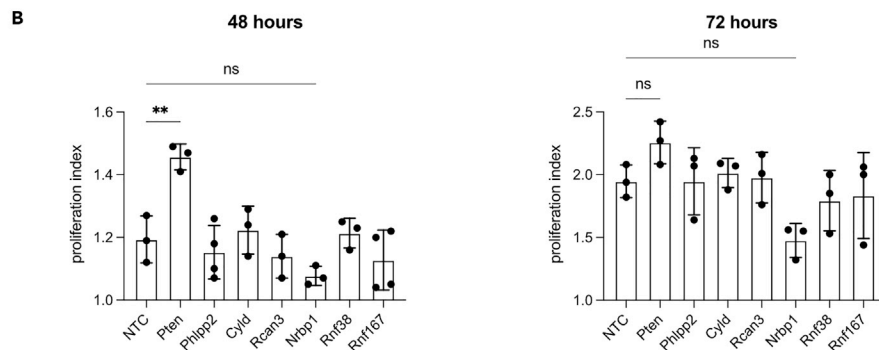
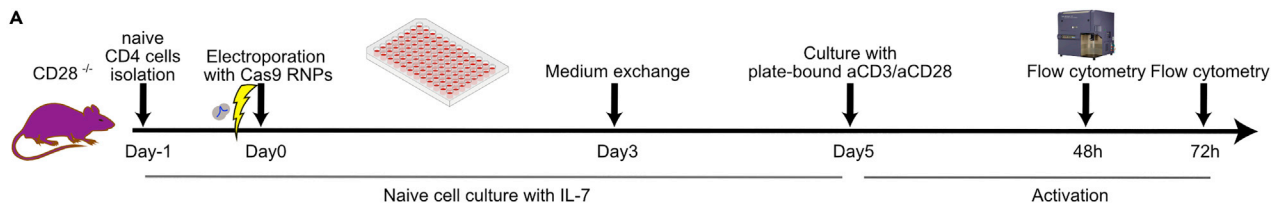


Figure 7. miR-17~92 target genes regulate discrete functions

(A) Schematic representation of Cas9 RNP electroporation experiments. Naive CD28^{-/-} CD4⁺ T cells were cultured with IL-7 to preserve a naive state for 5 days post-electroporation and activated for 48 or 72 h with plate-bound anti-CD3/anti-CD28. (B–E) proliferation index (B), MFI of CD25 (C), CD44 (D) and ICOS (E) after 48 and 72 h of activation. Data from 3 independent experiments. Error bars represent mean \pm SD, Dunnett's multiple comparison test; p values: ns = not significant, * <0.05 ** <0.002 *** <0.0002 **** <0.0001 .

Conversely, as illustrated above (Figure 6B) many direct targets were not only derepressed in T^{1792 Δ / Δ} but also in CD28^{-/-} cells. Several genes (e.g. *Rcan3*, *Nrbp1*, *Rnf38*, and *Rnf167*) were similarly derepressed in CD28^{-/-} and T^{1792 Δ / Δ} cells, expression was restored in "rescue" cells to levels similar to wt and even further repressed in T^{1792tg/tg} cells (Figure 6F). Others, such as *Phlpp2* and *Cyld* were clearly regulated by miR-17~92 but their expression differed in CD28^{-/-} and T^{1792 Δ / Δ} cells (Figure 6F). This suggests that these targets are sensitive to regulation by miR-17~92 and in multiple cases, their derepression observed in CD28^{-/-} T cells is largely attributed to reduced repression by miR-17~92. However, functional validation of candidate targets will be necessary.

miR-17~92 target genes regulate discrete functions

To understand the functional relevance of the empirically validated miR-17~92 targets (Table S1) we reasoned that genetically inactivating targets should have phenotypically similar effect as miR-17~92-mediated repression. We therefore chose to ablate candidate target genes in CD28^{-/-} T cells using CRISPR/Cas9. In order to be able to analyze a candidate gene's role during T cell activation we sought to delete candidate genes in naive T cells, i.e. before activation. To this end, we adapted a protocol to use CRISPR/Cas9 in naive CD4⁺ T cells (Seki and Rutz, 2018) (Figure 7A). We used a non-targeting control (NTC) crRNA as a negative control, included the well-validated miR-17~92 target *Pten* as a positive control and chose *Phlpp2*, *Cyld*, *Rcan3*, *Nrbp1*, *Rnf38*, and *Rnf167* (Figures 4F and 6F) to test our hypothesis. As readouts for potential phenotypic rescue we analyzed proliferation, CD25, CD44, and ICOS since these parameters were clearly restored in "rescue" T cells (Figures 1D–1F and 2B). In line with a previous report that genetic *Pten*-ablation in T cells removed the requirement for CD28 costimulation for proliferation (Buckler et al., 2006), we observed increased proliferation in cells electroporated with a *Pten*-targeting gRNA but not any of the other gRNAs (Figure 7B). This effect was clearly evident at 48 h but could no longer be detected at 72 h. Ablation of nuclear receptor binding protein 1 (*Nrbp1*) resulted in increased expression of CD25 after 72 h while the ablation of the other genes did not affect CD25 expression (Figure 7C). Furthermore, CD44 expression was increased by *Pten*-ablation at 48 and 72 h and by *Nrbp1*-ablation at 72 h. Finally, contrary to expectations, *Pten*-ablation resulted in decreased ICOS expression at 72 h. Thus, CRISPR/Cas-mediated ablation of individual target genes resulted in distinct phenotypic consequences. Deleting two individual miR-17~92 target genes in naive CD28^{-/-} CD4⁺ T cells increased 3 of the 4 tested parameters that were also rescued by transgenic miR-17~92 expression, suggesting that their repression by transgenic miR-17~92 in "rescue" T cells contributed to the phenotypic rescue observed. In contrast, the deletion of *Pten* resulted in two expected phenotypic consequences and one opposite to expectations. This suggests that ICOS upregulation observed in "rescue" T cells is not mediated by repression of *Pten* but rather an as yet unidentified miR-17~92 target gene. Together, these results support CRISPR/Cas-based gene deletion as a means to functionally validate candidate miRNA target genes and strongly suggest that miR-17~92-mediated repression of these targets is functionally relevant during T cell activation.

DISCUSSION

T cell activation depends on TCR and CD28 engagement to trigger complex molecular mechanisms including the activation of the PI3K, NF- κ B, and calcineurin/NFAT pathways. Intense research in the past decades uncovered many molecules that transmit TCR and CD28 signals (Esensten et al., 2016; Tian et al., 2015; Liu et al., 2018). Most studies focused on proteins as signaling intermediates but we and others previously reported that the combined engagement of TCR and CD28 also alters the expression of non-coding RNAs. Most miRNAs are downregulated after T cell activation but a few, including miR-17~92, remain relatively constant or are slightly induced (Bronevetsky et al., 2013; de Kouchkovsky et al., 2013). This suggests that miR-17~92 might be functionally relevant during T cell activation. We previously found that miR-17~92 was induced after combined stimulation of TCR and CD28 *in vitro* but not after TCR stimulation alone (de Kouchkovsky et al., 2013). Here, we found that TCR stimulation alone does induce miR-17 but that costimulation through CD28 synergistically further increased miR-17 expression. Even adding low CD28 costimulation resulted in higher miR-17 induction than high TCR stimulation alone. These findings are consistent with experiments using stimulation by the natural ligands CD80/CD86. Heterozygosity or

absence of CD80/CD86 on B cells resulted in a dose-dependent reduction in miR-17 induction in co-cultured T cells while deficiency or blockade of CTLA-4 resulted in increased miR-17 expression (Wang et al., 2015). Collectively, these studies demonstrate that TCR stimulation and costimulation/coinhibition by CD28 or CTLA-4 are intimately linked to miR-17~92 expression. Furthermore, stimulating T cells with antibodies directed to CD3 is sufficient to induce proliferation in $T^{1792tg/tg}$ T cells suggesting that transgenic miR-17~92 renders T cells CD28 costimulation independent (Xiao et al., 2008). Therefore, we set out to formally investigate if and how transgenic miR-17~92 was sufficient to substitute for the absence of CD28 and whether miR-17~92 was required for CD28-mediated T cell activation. We found an unexpectedly potent rescue effect both *in vitro* and *in vivo*. Many defects of CD28^{-/-} T cells were functionally compensated for by the miR-17~92 transgene. This is notable for two reasons. First, miR-17~92 is a non-coding RNA and second, miRNAs are negative regulators. Thus, overexpression of an inhibitory non-coding RNA was sufficient to enable T cell activation in the absence of CD28 costimulation.

To analyze the molecular mechanism by which miR-17~92 enabled T cell activation of CD28^{-/-} CD4⁺ T cells we first defined miR-17~92 target genes in CD28-sufficient CD4⁺ T cells before and after activation. RNA-seq analysis of T cells with miR-17~92 loss- or gain of function and sampled over a time course revealed that miR-17~92 mainly influenced the transcriptome after T cell activation, a finding consistent with the phenotypic analysis of *ex vivo* characterized naive T cells. There is an emerging notion that evidence of miRNA binding combined with differential gene expression in primary cells constitutes a precise approach to empirically define miRNA:target relationships (Gagnon et al., 2019; Hsin et al., 2018). We, therefore, employed this approach but refined it by combining EISA with AHC to discriminate whether differentially expressed gene clusters were primarily regulated transcriptionally or posttranscriptionally. This analysis provides a highly granular view of miRNA-mediated gene regulation. Specifically, pathway and regulon enrichment analysis revealed that miR-17~92 enhanced the calcineurin/NFAT pathway. Consistent with this, a gene cluster enriched for genes that positively correlated with miR-17~92 was mainly transcriptionally regulated and contained many genes known to be regulated by NFAT TF including genes for various CD4⁺ T cell subsets such as T_{FH} (*IL-21*) and T_H1 (*Tbx-21* and *IFN γ*). Experiments with pharmacologic CNIs, e.g. CsA, confirmed that miR-17~92 functionally promoted the calcineurin/NFAT pathway. Importantly, we demonstrated that the expression of genes we validated empirically as miR-17~92 targets were elevated in stimulated CD28^{-/-} T cells. In contrast, transgenic miR-17~92 partially restored the molecular program that was defective in CD28^{-/-} T cells. In particular, the expression of key NFAT-regulated genes found to be driven by miR-17~92 in CD28-sufficient T cells were restored by the transgene in CD28^{-/-} T cells. We conclude that during T cell activation miR-17~92 is required to repress this set of genes.

With the list of stringently defined miR-17~92 target genes, we set out to investigate the functional relevance of identified miRNA target genes. This is generally challenging because miRNAs bind to and regulate many genes and because the per gene repression is mostly modest (Baumjohann and Ansel, 2013). We previously addressed this using siRNA-mediated gene repression (Pua et al., 2016). Here, we reasoned that the disruption of genes that physiologically are to be repressed by miR-17~92 during T cell activation could partially restore defects of CD28-deficient T cells resulting in the gain of function (rescue) phenotypes. Indeed, some parameters that were rescued by transgenic miR-17~92 were also restored by the disruption of a single miR-17~92 target gene (*Pten*: proliferation; *Nrbp1*: CD25; see model in Figure S8) while others were restored by the disruption of more than one target (*Pten*, *Nrbp1*: CD44). For yet other targets we could not detect any functional relevance for the measured parameters (*Phlpp2*, *Cyld*, *Rcan3*, *Rnf38*, *Rnf167*). Importantly, due to the known dependency on the cellular context, the absence of a change in the assessed parameters does not exclude that repression of these genes may be relevant in a different context, timepoint, or for a function not assessed here (Lu et al., 2015; Hsin et al., 2018). For instance, it's interesting to note that CRISPR/Cas9-mediated disruption of *Pten* restored proliferation at the earlier time point but the effect waned with time. Similarly, we previously found that removing one copy of *Pten* was able to restore the defect observed in $T^{1792\Delta/\Delta}$ cells during early T_{FH} differentiation but not during later stages (Baumjohann et al., 2013). In addition, the disruption of *Pten* resulted in the opposite effect (decrease) than miR-17~92 transgene expression (increase) for ICOS expression. Therefore, although *Pten* is an important miR-17~92 target, others must be functionally relevant and remain to be identified. For instance, our limited CRISPR/Cas9 validation revealed that disrupting *Nrbp1* increased CD25 and CD44 expression suggesting that it regulates these important proteins. Interestingly, *Nrbp1* is a known tumor suppressor and *Nrbp1*-disruption increases CD44 and c-myc in the intestine of conditional KO mice (Wilson et al., 2012). These results suggest that *Nrbp1* is another negative regulator of T cell activation.

Together, these results clearly demonstrate that a single target is very unlikely to explain the phenotypic rescue observed in CD28^{-/-} T cells expressing transgenic miR-17~92. Rather, we propose that miR-17~92 represses a network of genes fulfilling distinct functions. A scaled up, targeted CRISPR/Cas9 screen could be used to identify regulators of T cell function. For instance, our data suggest that ICOS expression may be restrained by yet unknown miR-17~92 targets. In addition, not all target genes have binding sites for each of the miR-17~92 cluster's miRNAs. Therefore, such a screen could help to identify which miRNA of the cluster affects which function. As an example, we identify *Nrbp1* as a functionally relevant miR-17~92 target. Since it contains binding sites for miR-17 and miR-19 it is likely that one or both of these miRNAs are functionally relevant for its repression and consequently CD25 and CD44 regulation. However, investigation of the relevance of the respective binding sites needs separate validation experiments. Thus, our empirically validated target list provides a blueprint for an arrayed CRISPR/Cas9 screening approach to reveal new biologic insight. Expanding such a screen to additional readouts, e.g. IL-2 or Tbx21, might reveal the regulation of distinct functions by unexpected genes. Moreover, CRISPR/Cas9 screening in naive T cells could be useful beyond miRNA research, particularly in CD28^{-/-} T cells, e.g. to identify T cell negative regulators.

Our results are in line with limited experimental evidence that gene deletion can partially rescue CD28 deficiency. For instance, genetic deletion of Casitas B lymphoma-b protein (*Cbl-b*) or TRAF6 is sufficient to restore IL-2 production and proliferation in CD28^{-/-} T cells (Bachmaier et al., 2000; Chiang et al., 2000; King et al., 2006). However, neither IFN γ , IL-4 or ICOS expression nor GC formation was restored by *Cbl-b* deletion (Bachmaier et al., 2000; Chiang et al., 2000). Thus, while loss of *Cbl-b* uncoupled T cells from the strict requirement for CD28 costimulation, it could not restore all aspects of CD28-mediated costimulation suggesting that additional genes restrain T cell activation. As a group of genes, negative regulators impose a requirement for a costimulatory signal to actively remove these brakes to allow a productive T cell response. CD28 costimulation, therefore, serves a dual purpose by enhancing TCR signaling and simultaneously overcoming T cell repression (Paolino and Penninger, 2010; Buckler et al., 2006; Martinez-Llordella et al., 2013). Using *Pten*-deficient T cells it was previously shown that PTEN imposes a requirement for CD28 costimulation by setting a threshold for activation (Buckler et al., 2006). Here, we show that CRISPR/Cas-mediated *Pten* disruption can partially overcome defective proliferation and CD44 upregulation of CD28^{-/-} CD4⁺ T cells but negatively affects ICOS expression. In addition, we identify the tumor suppressor *Nrbp1* as an additional gene whose removal enables the the expression of important proteins in CD28^{-/-} CD4⁺ T cells. Moreover, our list of empirically validated miR-17~92 target genes contains several other known or suspected tumor suppressor genes. The growing list (e.g. *Pten*, *Phlpp2*, *Cyld*, *Nrbp1*) of tumor suppressors/negative regulators whose expression is controlled by miR-17~92 is noteworthy and suggests that these could all contribute to setting a threshold for T cell activation. Although it's remarkable that removing individual genes in CD28^{-/-} T cells is sufficient to restore specific functions, it's important to note that during T cell activation the inhibitors are not completely eliminated. Therefore, although experimental deletion can demonstrate that a given gene has the potential to act as a powerful negative regulator, its physiologic function is more delicate to uncover and complete deletion likely overestimates the contribution of the gene under investigation. To date, no single gene or pathway can explain the function of T cell activation and/or CD28 costimulation. More likely, multiple pathways need to be induced and multiple negative regulators need to be removed. It is conceivable that precise control of genetic programs is particularly important for an exponential process like clonal T cell expansion. Even minor changes in setting the T cell activation threshold or the rate of proliferation or survival could result in major consequences for the host organism. Since miRNAs fine-tune expression of many genes they are ideally suited to mediate controlled release from multiple restraining proteins preventing T cell activation (Bartel, 2018). Our findings greatly expand the list of high-confidence miR-17~92 targets with a suspected function in T cell activation and illustrate that miR-17~92 can exert complex regulation of the T cell transcriptome through direct and indirect gene regulation.

In summary, we propose a model (graphical abstract) in which miR-17~92 acts as a downstream mediator, modulator, and/or amplifier of the molecular program triggered by combined TCR/CD28 engagement serving as a gatekeeper of a network of restrainers of T cell activation and function. In this model, non-coding RNA-mediated direct repression of inhibitors indirectly supports the transcriptional induction of genes necessary for further T cell differentiation and function (e.g. CD44, IL-21, Tbx21,

IFN γ). Importantly, we not only show that transgenic miR-17~92 is largely sufficient to substitute for CD28-deficiency but that miR-17~92 is physiologically required to shape the transcriptome after CD28 costimulation and that miR-17~92 overexpression in CD28-sufficient T cells results in “super-costimulation.” In support of the proposed model, constitutive transgenic miR-17~92 expression leads to a lupus-like systemic autoimmune syndrome (Xiao et al., 2008), not unlike the ones observed in mice deficient in *Cbl-b*, *PTEN*, *TRAF6*, or *Cyld* (Bachmaier et al., 2000; Chiang et al., 2000; Suzuki et al., 2001; King et al., 2006; Reiley et al., 2007). Our results support the consideration of miR-17~92 or its target genes for pharmacologic intervention or for its integration into engineered cellular therapies.

Limitations of the study

Our study is limited in scope and by technical constraints concerning the mechanistic link between i) CD28, miR-17~92 and T cell activation, ii) miR-17~92 target validation as well as iii) relevance for other cells. We cannot definitively discern the relative functional relevance of miR-17~92 induced by TCR stimulation alone versus combined TCR and CD28 costimulation. This study did not address the molecular mechanism of miR-17~92 regulation in T cells. Although the presence of myc binding sites is suggestive of transcriptional regulation (O'Donnell et al., 2005), miRNA biogenesis can be controlled by extracellular cues and maturation of miR-17~92 is known to be regulated posttranscriptionally (Du et al., 2015). It will be important to identify the individual miRNAs of the cluster that regulate specific functions and to determine whether the expression of miR-17 (which we measured) corresponds to other miRNAs of the cluster, such as miR-18a, miR-19a, and miR-19b-1 that reportedly have an important function in T cells (Montoya et al., 2017; Simpson et al., 2014; Jiang et al., 2011). Together, future studies addressing these open questions will untangle the molecular connection between TCR stimulation/CD28 costimulation/T cell activation and miR-17~92 expression/function. For instance, such studies could address whether miR-17~92-deficient T cells receiving both TCR and costimulatory signal become anergic similar to costimulation-deficient T cells. With regards to miR-17~92 target validation the study did not address whether miR-17~92 increased calcineurin/NFAT activity through repression of a direct calcineurin inhibitor, e.g. *Rcan3*, or indirectly, e.g. through repression of a PI3K inhibitor, e.g. *Pten* or *Phlpp2*. Furthermore, a more comprehensive analysis of the repression of single or combinations of targets will be required but this will remain challenging since our results suggest a context and time-dependent regulation of multiple genes as observed for other miRNAs. Technically, the deletion efficiencies of the CRISPR/Cas9 approach varied, ranging from 13.4 to 28% (*Phlpp2*) to 65.5–84% (*Rnf167*) but 30–49% was sufficient to see phenotypic effects (*Nrbp1*) in this experiment. Interpretation of the results further needs to take into account that the inhibitors are not completely eliminated by miRNAs during T cell activation. Therefore, complete deletion likely overestimates the contribution of the gene under investigation. Finally, future studies need to determine whether T cell subsets that rely less on CD28 than naive T cells (e.g. memory and CD8⁺ T cells) display differential sensitivity to miR-17~92-mediated gene regulation or express more miR-17~92.

STAR★METHODS

Detailed methods are provided in the online version of this paper and include the following:

- KEY RESOURCES TABLE
- RESOURCE AVAILABILITY
 - Lead contact
 - Materials availability
 - Data and code availability
- EXPERIMENTAL MODEL AND SUBJECT DETAILS
 - Mice
- METHOD DETAILS
 - Organ isolation
 - Naïve CD4⁺ T cell isolation
 - Plate-bound CD4⁺ T cell activation
 - Proliferation assay with cell trace violet (CTV)
 - Enzyme-linked immunosorbent assay (ELISA)
 - FACS staining
 - LCMV Armstrong infection model

- Histology
- Adoptive transfer (AT) with subsequent LCMV infection
- RNA sequencing
- Regulon enrichment analysis
- AGO2 HITS-CLIP (AHC) data
- *In vitro* differentiation
- Seahorse
- Cyclosporin A (CsA) titration
- ImageStream
- Reverse transcription (RT) and quantitative PCR (qPCR)
- CRISPR/Cas9 editing of naïve CD4⁺ T cells
- **QUANTIFICATION AND STATISTICAL ANALYSIS**

SUPPLEMENTAL INFORMATION

Supplemental information can be found online at <https://doi.org/10.1016/j.isci.2022.105372>.

ACKNOWLEDGMENTS

We would like to thank the current and former lab members for scientific discussions; Daniel Pinschewer and Weldy Bonilla Pinschewer for advice on LCMV, reagents (GP61 peptide), and scientific discussions; Annaïse Jauch for providing LCMV Armstrong; Mihaela Zavolan and Ed Palmer for deep scientific discussions and critical comments on the article; members of the NCCR RNA & Disease for discussions; the University of Basel, the Basel University Hospital and Department of Biomedicine (DBM) for institutional support; the team from the DBM animal facility for animal husbandry; the DBM flow cytometry core team; Robert Ivanek from the DBM bioinformatics core; Philippe Demougin from the D-BSSE/DBM Genomics Facility Basel; Alexander Schmidt from the University of Basel Biozentrum Proteomics Core Facility for support and Marco Amsler, Caroline Schwenzel, H el ene Rossez, Giuseppina Capoferri and Corinne Engdahl-D emolli ere for technical assistance. Calculations were performed at sciCORE (<http://scicore.unibas.ch/>) scientific computing center at the University of Basel. This work was supported by grants of the Swiss National Science Foundation (SNSF Professorship PP00P3_144860 to LTJ), the National Institute of Allergy and Infectious Diseases of the National Institutes of Health, USA, under Award Number R56/R01AI106923 and the European Research Council (ERC) under the European Union's Horizon 2020 research and innovation program (grant agreement No. 818806) (to LTJ), and the National Heart, Lung, and Blood Institute of the National Institutes of Health, USA, under Award Numbers R01HL109102 and P01HL107202 (to KMA). The content of this study is solely the responsibility of the authors and does not necessarily represent the official views of the National Institutes of Health.

AUTHOR CONTRIBUTIONS

M.D. performed and analyzed most experiments; M.H. performed all CRISPR experiments, G.B. and C.H. helped to design and interpret metabolic experiments; R.M. performed qPCR experiments, provided scientific input, key experimental and infrastructure support; M.K. provided scientific input and experimental support; R.K. generated HITS-CLIP data; D.S. and J.R. performed the bioinformatic analysis with the help of J.G.; K.M.A. provided key scientific input and access to HITS-CLIP data; M.D. and L.T.J. designed the experiments, interpreted the data and discussed results; L.T.J. designed the study, obtained funding, supervised all experiments and wrote the article (MS) with the help of M.D. and M.H.; all authors approved the final MS.

DECLARATION OF INTERESTS

L.T.J. is a co-founder and board member of, holds equity in, and has a sponsored research agreement with Cimeio Therapeutics AG. M.D. and L.T.J. are inventors on a patent application related to the findings reported here.

Received: November 17, 2020

Revised: August 12, 2022

Accepted: October 12, 2022

Published: November 18, 2022

REFERENCES

- Acuto, O., and Michel, F. (2003). CD28-mediated co-stimulation: a quantitative support for TCR signalling. *Nat. Rev. Immunol.* 3, 939–951.
- Agarwal, V., Bell, G.W., Nam, J.W., and Bartel, D.P. (2015). Predicting effective microRNA target sites in mammalian mRNAs. *Elife* 4, e05005.
- Andrews, S. (2010). FastQC: a quality control tool for high throughput sequence data. <http://www.bioinformatics.babraham.ac.uk/projects/fastqc/>.
- Bachmaier, K., Krawczyk, C., Kozieradzki, I., Kong, Y.Y., Sasaki, T., Oliveira-Dos-Santos, A., Mariathasan, S., Bouchard, D., Wakeham, A., Itie, A., et al. (2000). Negative regulation of lymphocyte activation and autoimmunity by the molecular adaptor Cbl-b. *Nature* 403, 211–216.
- Barrat, F.J., Cua, D.J., Boonstra, A., Richards, D.F., Crain, C., Savelkoul, H.F., De Waal-Malefyt, R., Coffman, R.L., Hawrylowicz, C.M., and O'garra, A. (2002). In vitro generation of interleukin 10-producing regulatory CD4(+) T cells is induced by immunosuppressive drugs and inhibited by T helper type 1 (Th1)- and Th2-inducing cytokines. *J. Exp. Med.* 195, 603–616.
- Bartel, D.P. (2018). Metazoan microRNAs. *Cell* 173, 20–51.
- Baumjohann, D., and Ansel, K.M. (2013). MicroRNA-mediated regulation of T helper cell differentiation and plasticity. *Nat. Rev. Immunol.* 13, 666–678.
- Baumjohann, D., Kageyama, R., Clingan, J.M., Morar, M.M., Patel, S., De Kouchkovsky, D., Bannard, O., Bluestone, J.A., Matloubian, M., Ansel, K.M., and Jeker, L.T. (2013). The microRNA cluster miR-17 approximately 92 promotes TFH cell differentiation and represses subset-inappropriate gene expression. *Nat. Immunol.* 14, 840–848.
- Brinkman, E.K., Chen, T., Amendola, M., and Van Steensel, B. (2014). Easy quantitative assessment of genome editing by sequence trace decomposition. *Nucleic Acids Res.* 42, e168.
- Bronevetsky, Y., Villarino, A.V., Eisle, C.J., Barbeau, R., Barczak, A.J., Heinz, G.A., Kremmer, E., Heissmeyer, V., Mcmanus, M.T., Erle, D.J., et al. (2013). T cell activation induces proteasomal degradation of Argonaute and rapid remodeling of the microRNA repertoire. *J. Exp. Med.* 210, 417–432.
- Buckler, J.L., Walsh, P.T., Porrett, P.M., Choi, Y., and Turka, L.A. (2006). Cutting edge: T cell requirement for CD28 costimulation is due to negative regulation of TCR signals by PTEN. *J. Immunol.* 177, 4262–4266.
- Chen, W., Jin, W., Hardegen, N., Lei, K.J., Li, L., Marinos, N., McGrady, G., and Wahl, S.M. (2003). Conversion of peripheral CD4(+)CD25(-) naive T cells to CD4(+)CD25(+) regulatory T cells by TGF-beta induction of transcription factor Foxp3. *J. Exp. Med.* 198, 1875–1886.
- Chiang, Y.J., Kole, H.K., Brown, K., Naramura, M., Fukuhara, S., Hu, R.J., Jang, I.K., Gutkind, J.S., Shevach, E., and Gu, H. (2000). Cbl-b regulates the CD28 dependence of T-cell activation. *Nature* 403, 216–220.
- Crotty, S. (2011). Follicular helper CD4 T cells (TFH). *Annu. Rev. Immunol.* 29, 621–663.
- De Kouchkovsky, D., Esensten, J.H., Rosenthal, W.L., Morar, M.M., Bluestone, J.A., and Jeker, L.T. (2013). microRNA-17-92 regulates IL-10 production by regulatory T cells and control of experimental autoimmune encephalomyelitis. *J. Immunol.* 191, 1594–1605.
- Dobin, A., Davis, C.A., Schlesinger, F., Drenkow, J., Zaleski, C., Jha, S., Batut, P., Chaisson, M., and Gingeras, T.R. (2013). STAR: ultrafast universal RNA-seq aligner. *Bioinformatics* 29, 15–21.
- Doench, J.G., Fusi, N., Sullender, M., Hegde, M., Vaimberg, E.W., Donovan, K.F., Smith, I., Tothova, Z., Wilen, C., Orchard, R., et al. (2016). Optimized sgRNA design to maximize activity and minimize off-target effects of CRISPR-Cas9. *Nat. Biotechnol.* 34, 184–191.
- Dolz, M., Marone, R., and Jeker, L.T. (2021). Plasmid- or ribonucleoprotein-mediated CRISPR/Cas gene editing in primary murine T cells. *Methods Mol. Biol.* 2285, 255–264.
- Du, P., Wang, L., Sliz, P., and Gregory, R.I. (2015). A biogenesis step upstream of microprocessor controls miR-17 approximately 92 expression. *Cell* 162, 885–899.
- Edner, N.M., Carlesso, G., Rush, J.S., and Walker, L.S.K. (2020). Targeting co-stimulatory molecules in autoimmune disease. *Nat. Rev. Drug Discov.* 20, 82.
- Esensten, J.H., Helou, Y.A., Chopra, G., Weiss, A., and Bluestone, J.A. (2016). CD28 costimulation: from mechanism to therapy. *Immunity* 44, 973–988.
- Fabregat, A., Jupe, S., Matthews, L., Sidiropoulos, K., Gillespie, M., Garapati, P., Haw, R., Jassal, B., Korninger, F., May, B., et al. (2018). The reactome pathway knowledgebase. *Nucleic Acids Res.* 46, D649–D655.
- Ferguson, S.E., Han, S., Kelsoe, G., and Thompson, C.B. (1996). CD28 is required for germinal center formation. *J. Immunol.* 156, 4576–4581.
- Friedman, R.C., Farh, K.K.H., Burge, C.B., and Bartel, D.P. (2009). Most mammalian mRNAs are conserved targets of microRNAs. *Genome Res.* 19, 92–105.
- Gagnon, J.D., Kageyama, R., Shehata, H.M., Fasset, M.S., Mar, D.J., Wigton, E.J., Johansson, K., Litterman, A.J., Odorizzi, P., Simeonov, D., et al. (2019). miR-15/16 restrain memory T cell differentiation, cell cycle, and survival. *Cell Rep.* 28, 2169–2181.e4.
- Gaidatzis, D., Burger, L., Florescu, M., and Stadler, M.B. (2015a). Analysis of intronic and exonic reads in RNA-seq data characterizes transcriptional and post-transcriptional regulation. *Nat. Biotechnol.* 33, 722–729.
- Gaidatzis, D., Lerch, A., Hahne, F., and Stadler, M.B. (2015b). QuasR: quantification and annotation of short reads in R. *Bioinformatics* 31, 1130–1132.
- Garcia-Alonso, L., Holland, C.H., Ibrahim, M.M., Turei, D., and Saez-Rodriguez, J. (2019). Benchmark and integration of resources for the estimation of human transcription factor activities. *Genome Res.* 29, 1363–1375.
- Gross, G., and Eshhar, Z. (2016). Therapeutic potential of T cell chimeric antigen receptors (CARs) in cancer treatment: counteracting off-tumor toxicities for safe CAR T cell therapy. *Annu. Rev. Pharmacol. Toxicol.* 56, 59–83.
- Gubser, P.M., Bantug, G.R., Razik, L., Fischer, M., Dimeloe, S., Hoenger, G., Durovic, B., Jauch, A., and Hess, C. (2013). Rapid effector function of memory CD8+ T cells requires an immediate-early glycolytic switch. *Nat. Immunol.* 14, 1064–1072.
- Homet Moreno, B., Zaretsky, J.M., Garcia-Diaz, A., Tsoi, J., Parisi, G., Robert, L., Meeth, K., Ndoye, A., Rosenberg, M., Weeraratna, A.T., et al. (2016). Response to programmed cell death-1 blockade in a murine melanoma syngeneic model requires costimulation, CD4, and CD8 T cells. *Cancer Immunol. Res.* 4, 845–857.
- Hsin, J.P., Lu, Y., Loeb, G.B., Leslie, C.S., and Rudensky, A.Y. (2018). The effect of cellular context on miR-155-mediated gene regulation in four major immune cell types. *Nat. Immunol.* 19, 1137–1145.
- Hui, E., Cheung, J., Zhu, J., Su, X., Taylor, M.J., Wallweber, H.A., Sasmal, D.K., Huang, J., Kim, J.M., Mellman, I., and Vale, R.D. (2017). T cell costimulatory receptor CD28 is a primary target for PD-1-mediated inhibition. *Science* 355, 1428–1433.
- Jeker, L.T., and Bluestone, J.A. (2013). MicroRNA regulation of T-cell differentiation and function. *Immunol. Rev.* 253, 65–81.
- Jiang, S., Li, C., Olive, V., Lykken, E., Feng, F., Sevilla, J., Wan, Y., He, L., and Li, Q.J. (2011). Molecular dissection of the miR-17-92 cluster's critical dual roles in promoting Th1 responses and preventing inducible Treg differentiation. *Blood* 118, 5487–5497.
- Jin, H.Y., Oda, H., Lai, M., Skalsky, R.L., Bethel, K., Shepherd, J., Kang, S.G., Liu, W.H., Sabouri-Ghomi, M., Cullen, B.R., et al. (2013). MicroRNA-17~92 plays a causative role in lymphomagenesis by coordinating multiple oncogenic pathways. *EMBO J.* 32, 2377–2391.
- Kamphorst, A.O., Wieland, A., Nasti, T., Yang, S., Zhang, R., Barber, D.L., Konieczny, B.T., Daugherty, C.Z., Koenig, L., Yu, K., et al. (2017). Rescue of exhausted CD8 T cells by PD-1-targeted therapies is CD28-dependent. *Science* 355, 1423–1427.
- Kanehisa, M., Furumichi, M., Tanabe, M., Sato, Y., and Morishima, K. (2017). KEGG: new perspectives on genomes, pathways, diseases and drugs. *Nucleic Acids Res.* 45, D353–D361.
- Kang, S.G., Liu, W.H., Lu, P., Jin, H.Y., Lim, H.W., Shepherd, J., Fremgen, D., Verdin, E., Oldstone, M.B.A., Qi, H., et al. (2013). MicroRNAs of the

- miR-17 approximately 92 family are critical regulators of T(FH) differentiation. *Nat. Immunol.* **14**, 849–857.
- King, C.G., Kobayashi, T., Cejas, P.J., Kim, T., Yoon, K., Kim, G.K., Chiffolleau, E., Hickman, S.P., Walsh, P.T., Turka, L.A., and Choi, Y. (2006). TRAF6 is a T cell-intrinsic negative regulator required for the maintenance of immune homeostasis. *Nat. Med.* **12**, 1088–1092.
- Langmead, B., Trapnell, C., Pop, M., and Salzberg, S.L. (2009). Ultrafast and memory-efficient alignment of short DNA sequences to the human genome. *Genome Biol.* **10**, R25.
- Leach, D.R., Krummel, M.F., and Allison, J.P. (1996). Enhancement of antitumor immunity by CTLA-4 blockade. *Science* **271**, 1734–1736.
- Li, H., Handsaker, B., Wysoker, A., Fennell, T., Ruan, J., Homer, N., Marth, G., Abecasis, G., and Durbin, R.; 1000 Genome Project Data Processing Subgroup (2009). The sequence alignment/map format and SAMtools. *Bioinformatics* **25**, 2078–2079.
- Linterman, M.A., Denton, A.E., Divekar, D.P., Zvetkova, I., Kane, L., Ferreira, C., Veldhoen, M., Clare, S., Dougan, G., Espéi, M., and Smith, K.G. (2014). CD28 expression is required after T cell priming for helper T cell responses and protective immunity to infection. *Elife* **3**, e03180.
- Linterman, M.A., Rigby, R.J., Wong, R., Silva, D., Withers, D., Anderson, G., Verma, N.K., Brink, R., Hutloff, A., Goodnow, C.C., and Vinuesa, C.G. (2009). Roquin differentiates the specialized functions of duplicated T cell costimulatory receptor genes CD28 and ICOS. *Immunity* **30**, 228–241.
- Liu, Q., Zheng, J., Sun, W., Huo, Y., Zhang, L., Hao, P., Wang, H., and Zhuang, M. (2018). A proximity-tagging system to identify membrane protein-protein interactions. *Nat. Methods* **15**, 715–722.
- Loeb, G.B., Khan, A.A., Canner, D., Hiatt, J.B., Shendure, J., Darnell, R.B., Leslie, C.S., and Rudensky, A.Y. (2012). Transcriptome-wide miR-155 binding map reveals widespread noncanonical MicroRNA targeting. *Mol. Cell* **48**, 760–770.
- Lu, L.F., Gasteiger, G., Yu, I.S., Chaudhry, A., Hsin, J.P., Lu, Y., Bos, P.D., Lin, L.L., Zawislak, C.L., Cho, S., et al. (2015). A single miRNA-mRNA interaction affects the immune response in a context- and cell-type-specific manner. *Immunity* **43**, 52–64.
- Martinez, G.J., Hu, J.K., Pereira, R.M., Crampton, J.S., Togher, S., Bild, N., Crotty, S., and Rao, A. (2016). Cutting edge: NFAT transcription factors promote the generation of follicular helper T cells in response to acute viral infection. *J. Immunol.* **196**, 2015–2019.
- Martinez-Llordella, M., Esensten, J.H., Bailey-Bucktrout, S.L., Lipsky, R.H., Marini, A., Chen, J., Mughal, M., Mattson, M.P., Taub, D.D., and Bluestone, J.A. (2013). CD28-inducible transcription factor DEC1 is required for efficient autoreactive CD4+ T cell response. *J. Exp. Med.* **210**, 1603–1619.
- Moltzahn, F., Olshen, A.B., Baehner, L., Peek, A., Fong, L., Stöppler, H., Simko, J., Hilton, J.F., Carroll, P., and Belloch, R. (2011). Microfluidic-based multiplex qRT-PCR identifies diagnostic and prognostic microRNA signatures in the sera of prostate cancer patients. *Cancer Res.* **71**, 550–560.
- Montoya, M.M., Maul, J., Singh, P.B., Pua, H.H., Dahlström, F., Wu, N., Huang, X., Ansel, K.M., and Baumjohann, D. (2017). A distinct inhibitory function for miR-18a in Th17 cell differentiation. *J. Immunol.* **199**, 559–569.
- Mulero, M.C., Aubareda, A., Schlüter, A., and Pérez-Riba, M. (2007). RCAN3, a novel calcineurin inhibitor that down-regulates NFAT-dependent cytokine gene expression. *Biochim. Biophys. Acta* **1773**, 330–341.
- Nguyen, D.N., Roth, T.L., Li, P.J., Chen, P.A., Apathy, R., Mamedov, M.R., Vo, L.T., Tobin, V.R., Goodman, D., Shifrut, E., et al. (2020). Polymer-stabilized Cas9 nanoparticles and modified repair templates increase genome editing efficiency. *Nat. Biotechnol.* **38**, 44–49.
- O’connell, R.M., Rao, D.S., Chaudhuri, A.A., and Baltimore, D. (2010). Physiological and pathological roles for microRNAs in the immune system. *Nat. Rev. Immunol.* **10**, 111–122.
- O’donnell, K.A., Wentzel, E.A., Zeller, K.I., Dang, C.V., and Mendell, J.T. (2005). c-Myc-regulated microRNAs modulate E2F1 expression. *Nature* **435**, 839–843.
- Paolino, M., and Penninger, J.M. (2010). Cbl-b in T-cell activation. *Semin. Immunopathol.* **32**, 137–148.
- Pua, H., Steiner, D., Patel, S., Gonzalez, J., Ortiz-Carpena, J., Kageyama, R., Chiou, N.T., Gallman, A., De Kouchkovsky, D., Jeker, L., et al. (2016). MicroRNAs 24 and 27 suppress allergic inflammation and target a network of regulators of T helper 2 cell-associated cytokine production. *Immunity* **44**, 821–832.
- Reiley, W.W., Jin, W., Lee, A.J., Wright, A., Wu, X., Tewalt, E.F., Leonard, T.O., Norbury, C.C., Fitzpatrick, L., Zhang, M., and Sun, S.C. (2007). Deubiquitinating enzyme CYLD negatively regulates the ubiquitin-dependent kinase Tak1 and prevents abnormal T cell responses. *J. Exp. Med.* **204**, 1475–1485.
- Riha, P., and Rudd, C.E. (2010). CD28 co-signaling in the adaptive immune response. *Self. Nonself.* **1**, 231–240.
- Robinson, M.D., McCarthy, D.J., and Smyth, G.K. (2010). edgeR: a Bioconductor package for differential expression analysis of digital gene expression data. *Bioinformatics* **26**, 139–140.
- Robinson, M.D., and Oshlack, A. (2010). A scaling normalization method for differential expression analysis of RNA-seq data. *Genome Biol.* **11**, R25.
- Sandberg, R., Neilson, J.R., Sarma, A., Sharp, P.A., and Burge, C.B. (2008). Proliferating cells express mRNAs with shortened 3’ untranslated regions and fewer microRNA target sites. *Science* **320**, 1643–1647.
- Sansom, D.M., and Walker, L.S.K. (2013). CD28 costimulation: walking the immunological tightrope. *Eur. J. Immunol.* **43**, 42–45.
- Schaefer, C.F., Anthony, K., Krupa, S., Buchoff, J., Day, M., Hannay, T., and Buetow, K.H. (2009). PID: the pathway interaction database. *Nucleic Acids Res.* **37**, D674–D679.
- Schneider, C.A., Rasband, W.S., and Eliceiri, K.W. (2012). NIH Image to ImageJ: 25 years of image analysis. *Nat. Methods* **9**, 671–675.
- Seki, A., and Rutz, S. (2018). Optimized RNP transfection for highly efficient CRISPR/Cas9-mediated gene knockout in primary T cells. *J. Exp. Med.* **215**, 985–997.
- Shahinian, A., Pfeffer, K., Lee, K.P., Kündig, T.M., Kishihara, K., Wakeham, A., Kawai, K., Ohashi, P.S., Thompson, C.B., and Mak, T.W. (1993). Differential T cell costimulatory requirements in CD28-deficient mice. *Science* **261**, 609–612.
- Shang, W., Jiang, Y., Boettcher, M., Ding, K., Mollenauer, M., Liu, Z., Wen, X., Liu, C., Hao, P., Zhao, S., et al. (2018). Genome-wide CRISPR screen identifies FAM49B as a key regulator of actin dynamics and T cell activation. *Proc. Natl. Acad. Sci. USA* **115**, E4051–E4060.
- Simpson, L.J., Patel, S., Bhakta, N.R., Choy, D.F., Brightbill, H.D., Ren, X., Wang, Y., Pua, H.H., Baumjohann, D., Montoya, M.M., et al. (2014). A microRNA upregulated in asthma airway T cells promotes TH2 cytokine production. *Nat. Immunol.* **15**, 1162–1170.
- Steiner, D.F., Thomas, M.F., Hu, J.K., Yang, Z., Babiarz, J.E., Allen, C.D.C., Matloubian, M., Belloch, R., and Ansel, K.M. (2011). MicroRNA-29 regulates T-box transcription factors and interferon-gamma production in helper T cells. *Immunity* **35**, 169–181.
- Subramanian, A., Tamayo, P., Mootha, V.K., Mukherjee, S., Ebert, B.L., Gillette, M.A., Paulovich, A., Pomeroy, S.L., Golub, T.R., Lander, E.S., and Mesirov, J.P. (2005). Gene set enrichment analysis: a knowledge-based approach for interpreting genome-wide expression profiles. *Proc. Natl. Acad. Sci. USA* **102**, 15545–15550.
- Suzuki, A., Yamaguchi, M.T., Ohteki, T., Sasaki, T., Kaisho, T., Kimura, Y., Yoshida, R., Wakeham, A., Higuchi, T., Fukumoto, M., et al. (2001). T cell-specific loss of Pten leads to defects in central and peripheral tolerance. *Immunity* **14**, 523–534.
- Tian, R., Wang, H., Gish, G.D., Petsalaki, E., Pasculescu, A., Shi, Y., Mollenauer, M., Bagshaw, R.D., Yosef, N., Hunter, T., et al. (2015). Combinatorial proteomic analysis of intercellular signaling applied to the CD28 T-cell costimulatory receptor. *Proc. Natl. Acad. Sci. USA* **112**, E1594–E1603.
- Vaeth, M., Maus, M., Klein-Hessling, S., Freinkman, E., Yang, J., Eckstein, M., Cameron, S., Turvey, S.E., Serfling, E., Berberich-Siebelt, F., et al. (2017). Store-operated Ca(2+) entry controls clonal expansion of T cells through metabolic reprogramming. *Immunity* **47**, 664–679.e6.
- Vigne, S., Palmer, G., Lamacchia, C., Martin, P., Talabot-Ayer, D., Rodriguez, E., Ronchi, F., Sallusto, F., Dinh, H., Sims, J.E., and Gabay, C. (2011). IL-36R ligands are potent regulators of dendritic and T cells. *Blood* **118**, 5813–5823.

Walker, L.S., Gulbranson-Judge, A., Flynn, S., Brocker, T., Raykundalia, C., Goodall, M., Förster, R., Lipp, M., and Lane, P. (1999). Compromised OX40 function in CD28-deficient mice is linked with failure to develop CXC chemokine receptor 5-positive CD4 cells and germinal centers. *J. Exp. Med.* 190, 1115–1122.

Wang, C.J., Heuts, F., Ovcinnikovs, V., Wardzinski, L., Bowers, C., Schmidt, E.M., Kogimtzis, A., Kenefeck, R., Sansom, D.M., and Walker, L.S.K. (2015). CTLA-4 controls follicular helper T-cell differentiation by regulating the strength of CD28

engagement. *Proc. Natl. Acad. Sci. USA* 112, 524–529.

Wilson, C.H., Crombie, C., Van Der Weyden, L., Poulogiannis, G., Rust, A.G., Pardo, M., Gracia, T., Yu, L., Choudhary, J., Poulin, G.B., et al. (2012). Nuclear receptor binding protein 1 regulates intestinal progenitor cell homeostasis and tumour formation. *EMBO J.* 31, 2486–2497.

Wu, D., and Smyth, G.K. (2012). Camera: a competitive gene set test accounting for

inter-gene correlation. *Nucleic Acids Res.* 40, e133.

Xiao, C., and Rajewsky, K. (2009). MicroRNA control in the immune system: basic principles. *Cell* 136, 26–36.

Xiao, C., Srinivasan, L., Calado, D.P., Patterson, H.C., Zhang, B., Wang, J., Henderson, J.M., Kutok, J.L., and Rajewsky, K. (2008). Lymphoproliferative disease and autoimmunity in mice with increased miR-17-92 expression in lymphocytes. *Nat. Immunol.* 9, 405–414.

STAR★METHODS

KEY RESOURCES TABLE

REAGENT or RESOURCE	SOURCE	IDENTIFIER
Antibodies		
Rat anti-mouse CD4 clone GK1.5 or RM4-5	Biolegend	Cat#100423, 100532
Rat anti-mouse/human CD44 clone IM7	Biolegend	Cat#103032, 103008
Rat anti-mouse CD62L clone MEL-14	Biolegend	Cat#104412
Armenian Hamster anti-mouse CD69 clone H1.2F3	Biolegend	Cat#104537
Rat anti-mouse CD25 clone PC61	Biolegend	Cat#102016
Mouse anti-mouse Tbet clone 4B10	Biolegend	Cat#644810
Rat anti-mouse IFN γ clone XMG1.2	Biolegend	Cat#505813
Rat anti-mouse IL-17a clone TC11-18H10.1	Biolegend	Cat#506904
Mouse anti-mouse Ror γ t clone Q31-378	BD BioScience	Cat#562684
Rat anti-mouse Foxp3 clone FJK-16s	eBioscience	Cat#17-5773-82
Armenian Hamster anti-mouse Fas (CD95) clone Jo2	BD BioScience	Cat#554257
Rat anti-mouse anti-GL-7 clone GL7	Biolegend	Cat#144612, 144610
Mouse anti-mouse anti-Bcl-6 clone K112-91	BD BioScience	Cat#561522
Armenian Hamster anti-mouse anti-ICOS (CD278) clone C398.4A	Biolegend	Cat#313525
Rat anti-mouse CXCR5 (CD185) clone SPRCL5	Biolegend	Cat#145513
Rat anti-mouse PD-1 (CD279) clone 29F.1A12	Biolegend	Cat#135216
Rat anti-mouse B220 clone RA3-6B2	Biolegend, Tonbo	Cat#103229, 20-0452-U100
Rat anti-mouse CD19 clone 1D3	Biolegend	Cat#115555, 115522
Armenian Hamster anti-mouse CD3e clone 145-2C11	Biolegend	Cat#100319, 100309
Rat anti-mouse anti-IL-2 clone JES6-5H4	Biolegend	Cat#503808
Rat anti-mouse V α 2 clone B20.1	Biolegend,	Cat#127816
Armenian Hamster anti-mouse anti-V β 8.3 clone 1B3.3	BD BioScience	Cat#553664
Armenian Hamster anti-mouse CD3 clone 2C11 (for coating)	BioXcell	Cat#BP0001-1
Armenian Hamster anti-mouse CD28 clone PV-1 (for coating)	BioXcell	Cat#BE0015-5
Rat anti-mouse CD16/CD32 clone 2.4G2 (for blocking)	BioXcell	Cat#BE0307
anti-IL4 clone 11B11	UCSF	AM039-PURE-B25
anti-IFN γ clone XMG1.2	UCSF	AM034-PURE-B25
anti-IL12/23 clone C17.8	UCSF	AM037-PURE-B25
Goat anti-mouse IgG1	ThermoFisher	A21240
Mouse anti-mouse NFATC2 clone 25A10.D6.D2	ThermoFisher	MA1-025
Bacterial and virus strains		
LCMV Armstrong	Annaise Jauch	N/A
Chemicals, peptides, and recombinant proteins		
FCS for medium	Atlanta	S11150
HEPES	SIGMA	H0887
Sodium pyruvate	Gibco	11360-039

(Continued on next page)

Continued

REAGENT or RESOURCE	SOURCE	IDENTIFIER
non-essential amino acids	Gibco	11140-050
Glutamax	Gibco	35050-038
0.1% 2-Mercaptoethanol	Gibco	31350-010
FCS for FACS buffer	Milian	S0750
NaN ₃	SIGMA	S2002-5G
NH ₄ Cl	SIGMA	A9434-500G
NaHCO ₃	SIGMA	S5761-500G
Proteinase K	Promega	V3021
TE buffer	SIGMA	93283-100ML
Fixation/Permeabilization Concentrate	invitrogen	00-5123-43
Fixation/Permeabilization Diluent	invitrogen	00-5223-5
Permeabilization Buffer 10X	eBioscience	00-8333-56
OneComp eBeads	invitrogen	01-111-42
TRI Reagent	Sigma-Aldrich	T9424-200ML
1-Bromo-3-chloropropane	Sigma-Aldrich	B9673-200ML
M-MLV Reverse Transcriptase	Sigma-Aldrich	M1302-40KU
TaqMan™ MicroRNA Reverse Transcription Kit	ThermoFisher	4366597
TaqMan™ Fast Universal PCR Master Mix (2X), no AmpErase™ UNG	ThermoFisher	4364103
TaqMan Gene Expression Assays RCAN3	ThermoFisher	4351372
TaqMan Gene Expression Assays 18S	ThermoFisher	4331182
MicroAmp™ Fast Optical 96-Well Reaction Plate, 0.1 mL	ThermoFisher	4346907
EasySep naïve CD4 ⁺ T cell Isolation Kit	STEMCELL	19765A
CellTAK adhesive	Corning	354241
Seahorse XFe96/XF96 FluxPak (18 cartr.)	SeahorseBiotech	PN 102416-100
Glucose-free unbuffered RPMI	SIGMA	R6504-10X1L
Oligomycin	SIGMA	495445
FCCP	SIGMA	C2920
Rotenone	SIGMA	R8875
D-(+)-Glucose	Sigma-Aldrich	G7021
Fixable Viability Dye eF780	eBioscience	65-0865-14
Cell Trace Violet (CTV)	ThermoFisher	C34557
Phorbol 12-Myristate 13-Acetate (PMA)	Sigma	P1585
Ionomycin	Sigma	10634-1MG
Brefeldin A (BFA)	Sigma	B7651-5MG
GP-64	Neosystem	SP991567B
IL-2	R&D	202-IL
Retinoic acid	Sigma	R2625
rhTGFβ	R&D	P01137
IL-6	R&D	406ML
IL-7	R&D	407-ML-005
Cyclosporin A (CsA)	Sigma	30024
DAPI	Sigma	10236276001
IL-12	R&D	419ML
TMB	BD	555214

(Continued on next page)

Continued

REAGENT or RESOURCE	SOURCE	IDENTIFIER
Cas9 nuclease	QB3 MacroLab, UC Berkeley	N/A
Sodium deoxycholate	Thermo Scientific	89904
TRIS	Sigma,	T6791
TCEP	Sigma	646547-10x1ml
PR-Sulfonate Cartridges	PreOmics	N/A
Microplate BCA Protein Assay Kit	Thermo-Pierce	23252
Chloroacetamide	Sigma	C0267-100G
TFA	Pierce/Thermo	28904
Lysin-C	Wako	125-05061
Porcine Trypsin	Promega	V5113
2-Propanol	Sigma-Aldrich	19516-500ML
Ethanol	Sigma-Aldrich	51976-500ML-F
Ammonium hydroxide solution	Sigma-Aldrich	17093-1L
HPLC water	Chemie Brunswick	W/0106/17
Acetonitrile	Thermo Scientific	A955-212
Formic acid	Sigma	94318-50ml
Poly-L-glutamic acid sodium salt (PGA)	Sigma	P4761
QuickExtract	Lucigen	QE09050

Critical commercial assays

ELISA MAX mouse IL-2 set	BioLegend	431002
Nunc-Immuno™ MicroWell™ 96 well solid plates	SIGMA	M9410-1CS
Zymol Directzol kit	ZymoResearch	R2060

Deposited data

Raw and analyzed data	This paper	N/A
Mouse reference genome	UCSC	MM10
Generated data GEO accession number	This paper	GSE140568

Experimental models: Organisms/strains

Mir17-92<tm1.1Tyj>/J (crossed to CD4cre, T ^{1792Δ/Δ})	Dr. Bluestone, UCSF	N/A
C57Bl/6-Gt(ROSA)26Sor<tm3(CAG-MIRN17-92,-EGFP)Rsky>/J (crossed to CD4cre, T ^{1792tg/tg})	The Jackson Laboratory	stock number 008517
B6.Cg-Tg(Cd4-cre)1Cwi/BfluJ	The Jackson Laboratory	stock number 022071
B6.129S2-Cd28tm1Mak/J	SWIMR	N/A
B6-Tg(TCRGP13)1 BrI	SWIMR	N/A

Oligonucleotides

Rcan3 crRNA GAGAAATACGAACTGCACGC	IDT	N/A
Cyld crRNA GTTGGCAATTACCAACTGTG	IDT	N/A
Pten crRNA CCTCCAATTCAGGACCCACG	IDT	N/A
Phlpp2 crRNA TTGTACTGCAGCAGACGA	IDT	N/A
Nrbp1 crRNA AAACTGCTTAAGACTCCCAG	IDT	N/A
Rnf38 crRNA CTCCTACACGGTAACTACGG	IDT	N/A

(Continued on next page)

Continued

REAGENT or RESOURCE	SOURCE	IDENTIFIER
Rnf167 crRNA GGAATGAGGTAATAGCCCAA	IDT	N/A
Negative control crRNA#2	IDT	1072545
tracrRNA	IDT	1072532
fwd primer Rcan3 TCAGCCACTGAATGACGTAGTAG	Microsynth	N/A
rev primer Rcan3 GCGTCTGCGTGATTTTCTGT	Microsynth	N/A
Fwd primer Cyld CCTGTGGAGCCAAGAGAAAGT	Microsynth	N/A
Rev primer Cyld TCCTGGGGTCTATCCTGAGAA	Microsynth	N/A
Fwd primer Pten AGAAGTCCTTACATGGGTTGGT	Microsynth	N/A
Rev primer Pten GCTTTAAGCAAAGGTCTGTGGT	Microsynth	N/A
Fwd primer Phlpp2 GTGTCTGCCCTGGCTATGGA	Microsynth	N/A
Rev primer Phlpp2 GTGGTCCAGGAAGGAGTAACAG	Microsynth	N/A
Fwd primer Nrbp1 GTTCTACTGTGCTCTTAAGCC	Microsynth	N/A
Rev primer Nrbp1 CCCCTAGTCTTGTCTATCCC	Microsynth	N/A
Fwd primer Rnf38 TACTTGAGCTACCTCCCCCG	Microsynth	N/A
Rev primer Rnf38 TCAGTTGGAAGTGAAGCTACAAA	Microsynth	N/A
Fwd primer Rnf167 AAGCGCAGAGTACCTACGAG	Microsynth	N/A
Rev primer Rnf167 TCCCCTTACCGATCCAGTC	Microsynth	N/A

Software and algorithms

FlowJo 10.6.0	BD	N/A
Prism 8.2.0	GraphPad	N/A
IDEAS software v6.2	Merck	N/A
TIDE	Brinkman et al. (2014)	https://tide.nki.nl/
Fragment Analyzer	Advanced Analytical	N/A
FastQC tool version 0.11.5	Andrews (2010)	N/A
STAR version 2.5.2a	Dobin et al. (2013)	N/A
R software version 3.5	R Core Team 2015	http://www.R-project.org/
R Bioconductor package QuasR version 1.18	Gaidatzis et al., 2015b	N/A
R Bioconductor package edgeR version 3.24.3	Robinson et al. (2010)	N/A
ImageJ	Schneider et al. (2012)	https://imagej.nih.gov/ij/

Other

Sequence data, analyses, and resources related to the RNA-sequencing of T ^{1792Δ/Δ} , wt, T ^{1792tg/tg}	This paper	N/A
---	------------	-----

(Continued on next page)

Continued

REAGENT or RESOURCE	SOURCE	IDENTIFIER
Sequence data, analyses, and resources related to the RNA-sequencing of CD28 ^{-/-} , rescue, T ^{1792Δ/Δ} , wt, T ^{1792tg/tg}	This paper	N/A
Curated gene set collection of the Molecular Signature Database (MSigDB v6.0)	Subramanian et al. (2005)	N/A

RESOURCE AVAILABILITY

Lead contact

Further information and requests for resources should be directed to and will be fulfilled by the lead contact, Lukas Jeker (lukas.jeker@unibas.ch).

Materials availability

This study did not generate new unique reagents.

Data and code availability

Data generated in this study are available at GEO under accession number GEO:GSE140568.

Code is accessible at this location: <https://gitlab.com/JekerLab/mir17-92-rescues-cd28-deficient-cd4-t-cells>. Any additional information required to reanalyze the data reported in this paper is available from the [lead contact](#) upon request.

EXPERIMENTAL MODEL AND SUBJECT DETAILS

Mice

All animal work was performed in accordance with the federal and cantonal laws of Switzerland. Protocols were approved by the Animal Research Commission of the Canton of Basel-Stadt, Switzerland. Most of the mouse lines were imported from the JAX laboratory as indicated in the [key resources table](#). T^{1792Δ/Δ} mice were imported from the laboratory of Dr. Bluestone (UCSF). Rescue SM⁺ mice were obtained by crossing the rescue strain to other transgene lines in house so that their precise genetic origin is difficult to determine. As for the transfer cells, we used SM CD45.1⁺ wt cells imported from SWIMR. All other mouse lines were crossed to CD45.2 expression. Cre negative littermates (from T^{1792tg/tg} or T^{1792Δ/Δ}) were used as wt controls, and cre negative littermates from the rescue strain were used as CD28ko. 6–8 week old females and males were used for all experiments.

METHOD DETAILS

Organ isolation

Organs were obtained after CO₂ euthanization and kept on ice until processing. Mesenteric lymph nodes (LN), peripheral LN (inguinal, axillary, brachial, six cervical) and spleen were taken for most of the experiments. Spleens were injected with 0.5 mL ACK lysis buffer (0.155 M NH₄Cl, 200 μL 0.5 M EDTA pH = 8.0, 0.012 M NaHCO₃ pH 7.2) for erythrolysis before processing. The organs were meshed with 0.4 μm filters to obtain single cell suspensions which were then washed with FACS buffer (2% heat-inactivated FCS in PBS, for stainings add 0.02% NaN₃). Cells were centrifuged at 4°C, 5 min at a speed of 370 g for most washing procedures.

Naïve CD4⁺ T cell isolation

Naïve CD4⁺ T cells were isolated from cell suspensions with pooled lymph nodes and spleen. Isolation was performed with StemCell mouse naïve CD4⁺ T cell isolation kit according to manufacturer's instructions. In brief, the cell suspensions were incubated with rat serum and CD4⁺ isolation antibody for 7.5 minutes, then with memory depletion antibody for 2.5 minutes, and in the end with magnetic beads for another 2.5 minutes before incubating with the isolation magnet for 2.5 minutes. The resulting untouched naïve CD4⁺ T cells were then washed with FACS buffer, and purity was routinely checked with a staining for CD4⁺, CD44⁻ and viability.

Plate-bound CD4⁺ T cell activation

Plates were coated over night with 0.2 µg anti-CD28 and 0.5 µg anti-CD3 per mL PBS for most of the experiments (low stimulation as according to (Baumjohann et al., 2013)). We used 1 mL/well for 24 well plates and 0.2 mL/well for 96 well plates. Before plating of the cells, plates were washed with PBS. We plated 2×10^5 naïve CD4⁺ T cells per well in 96 well flat-bottom in 200 µL medium. For 24 well plates, 2×10^6 naïve CD4⁺ T cells per mL medium in 1 mL medium were plated. Complete T cell medium (RPMI-1640 Medium, 10% FCS, 1% HEPES, 1% non-essential amino acids, 1% Glutamax, 0.1% 2-Mercaptoethanol) was supplemented with 50U IL-2/mL. Cells were cultured at 37°C, 5% CO₂ for 24 h or longer depending on the purpose of the experiment as indicated in figure legends.

Proliferation assay with cell trace violet (CTV)

Freshly isolated naïve CD4⁺ T cells were washed with PBS. 1 µL of Cell Trace stock solution (dissolved in DMSO according to the manufacturer's instructions) was then used per mL PBS for 10×10^6 cells. Cells were incubated at 37°C for 20 minutes, then 5x the original staining volume of normal T cell culture medium was added for 5 minutes to remove residual dye. Cells were washed and plated in complete culture medium supplied with 50U IL-2 per mL for 48 h.

Enzyme-linked immunosorbent assay (ELISA)

IL-2 secretion was addressed in 48 h culture supernatants from cells that were plated in pre-coated wells in complete T cell medium without IL-2. IL-2 ELISA was performed with the BioLegend ELISA MAX mouse IL-2 set according to the manufacturer's instructions. After the last washing step, TMB substrate was added for the readout. Absorbance was measured with an ELISA plate reader (Synergy H1 Hybrid Reader, BioTek) at 450 nm as well as 570 nm wavelength, and normalized to wild type control samples that were run in the same experiment.

FACS staining

Generally, cells were stained for viability with viability dye eFluor780 in PBS for 20 min at 4°C and then washed with PBS or FACS buffer. Non-specific binding was blocked with anti-CD16/anti-CD32 0.5 mg/mL on ice for 10 minutes. Surface staining was performed in FACS buffer for 20–30 minutes at 4°C. In intracellular staining or LCMV experiments, cell fixation was performed with Fix-Perm for 20 minutes on 4°C (1 h for LCMV experiments). Intracellular staining was done in permeabilization buffer for 1 h at 4°C. Activation status of the cells was assessed by staining and gating for singlets/lymphocytes/viable cells/CD4⁺ and early activation marker CD25/CD69 as well as CD44/CD62L expression. Blasting of lymphocytes was addressed by pre-gating on singlets/viable cells. For cytokine staining after *in vitro* differentiation or *ex vivo* e.g., for IL-2 staining, cells were stimulated with 50 ng/mL PMA, 500 ng/mL Ionomycin and 10 µg/mL Brefeldin A (BFA) for 3 h at 37°C before staining. Data was acquired with an LSR Fortessa (BD) and analyzed with FlowJo.

LCMV Armstrong infection model

Mice were infected with 2×10^5 PFU LCMV-Armstrong strain i.p. with U-100 insulin syringes (0.30 mm (30G) x 8 mm). Eight days post infection the spleens were harvested for staining. We gated for singlets/lymphocytes/viable cells/CD3⁺CD4⁺ to look at CD44 expression, and moreover we addressed T_{FH} cells by the co-expression of key markers Bcl-6, PD-1, ICOS and CXCR5. We gated for singlets/lymphocytes/viable cells/CD19⁺B220⁺ to look at GC B cells expressing Fas and GL-7. Re-stimulation of splenocytes was performed in flat bottom 96 well plates with 1 µg/mL LCMV-specific peptide GP-64 in comparison to polyclonal 50 ng/mL PMA, 500 ng/mL Ionomycin stimulation for one hour, then 10 µg/mL Brefeldin A was added for another three hours before staining. We then gated for T_H1 cells using singlets/lymphocytes/viable cells/CD3⁺CD4⁺ and finally looking at Tbx21/IFNγ expression. All *in vivo* experiments were performed blinded with assignment of animal numbers after data analysis.

Histology

Spleens were embedded in cryo embedding medium and frozen on dry ice before storage at –80°C. Sections were cut at a thickness of 6 µm and dried on air. Single sections were then fixed with acetone for 5 minutes and circled with PAP pen. Staining for CD19, CD4 and GL-7 was performed in FACS buffer with anti-CD16/anti-CD32 in a wet chamber at 4°C overnight. Slides were then washed with PBS on a shaker

for 15 minutes before drying and mounting. Imaging was performed with a 20x objective on a Nikon Ti2 microscope and analyzed with ImageJ version 2.0.0.

Adoptive transfer (AT) with subsequent LCMV infection

Naïve SMARTA⁺ CD4⁺ T cells from wt, CD28^{-/-} and rescue mice were isolated transferred into CD28^{-/-} recipients. Each recipient received 1*10⁵ cells in 100 µL PBS i.v. The recipients were infected with 2*10⁵ PFU LCMV Armstrong i.p. two days after cell transfer. Eight days after infection, the mesenteric and peripheral LN as well as the spleen were analyzed separately for the presence of Vα2⁺Vβ8.3⁺ T cells (pre-gated on singlets/lymphocytes/viable cells/CD4⁺), and these cells were further characterized for their CD44 expression. One CD28^{-/-} mouse that did not receive donor cells was used as a negative control in each experiment to display the recipient-intrinsic Vα2⁺Vβ8.3⁺ population.

RNA sequencing

For any experiment involving RNA, cells were washed with PBS before counting and the RNA was kept on ice during the experiments, storage at -80°C. All pipetting was performed with filter-tips and RNase-free tubes. All procedures for the extractions were performed at the facilities with materials, protocols and supervision of the facility experts. For RNA sequencing, 2.5*10⁵ cells were washed with PBS and resuspend in 200 µL TRI Reagent. RNA was extracted from Trizol-samples with a Zymo Direct-zol kit which includes DNase treatment. Quality control was run with a Bioanalyzer. RNA quality was assessed with a Fragment Analyzer (Advanced Analytical) and RNA-seq library preparation was performed using Illumina Truseq stranded kit. Sequencing was performed on an Illumina NexSeq 500 machine to produce single-end 76-mers reads. All steps were performed at the Genomics Facility Basel (ETH Zurich).

Read quality was assessed with the FastQC tool (version 0.11.5). Reads were mapped to the mouse genome (UCSC version mm10) with STAR (version 2.5.2a) (Dobin et al., 2013) with default parameters, except filtering out reads mapping to more than 10 genomic locations (outFilterMultimapNmax = 10), reporting only one hit in the final alignment for multimappers (outSAMmultNmax = 1) and filtering reads without evidence in the spliced junction table (outFilterType = "BySJout").

All subsequent gene expression data analysis was performed using the R software (version 3.5). Read alignment quality was evaluated using the qQCReport function of the R Bioconductor package QuasR (version 1.18). Gene expression was quantified using the qCount function of QuasR (Gaidatzis et al., 2015b) as the number of reads (5'ends) overlapping with the exons of each gene assuming an exon union model (using the UCSC knownGenes annotation downloaded on 2015-12-18). To quantify intronic expression levels, exonic coordinates were extended by 10 bp on each side of the exons, and for each gene the resulting read count was subtracted to the read count obtained on the whole gene (extended by 10 bp on each side).

The R Bioconductor package edgeR (version 3.28) (Robinson et al., 2010) was used for differential gene expression analysis. Between samples normalization was done using the TMM method (Robinson and Oshlack, 2010). Only genes with CPM (counts per million reads mapped) values more than 1 in at least 4 samples (the number of biological replicates) were retained. Principal component analysis (PCA) was performed on the log-transformed normalized CPM values. An generalized linear model including a genotype effect, an activation effect, and a replicate effect (nested within genotype) was fitted to the raw counts (function glmFit), and differential expression was tested using likelihood ratio tests (function glmLRT). p-values were adjusted by controlling the false-discovery rate (Benjamini-Hochberg method) and genes with a FDR lower than 1% were considered differentially expressed.

To select a restricted list of most likely miRNA targets for each seed family, we restricted the genes to those with a conserved 3'UTR seed match (using TargetScan (Friedman et al., 2009)), and a coverage of more than 5 AHC reads. We additionally restricted the list by using differential expression criteria from the first RNA-seq dataset: genes should be significantly differentially expressed between T^{1792tg/tg} and wt, as well as between T^{1792Δ/Δ} and wt, with fold-changes in the expected directions; using intronic read counts, genes should not be significantly differentially expressed in the same comparison, at an increased FDR threshold of 10%.

Gene set enrichment analysis was performed with the function camera (Wu and Smyth, 2012) from the limma package (version 3.42; using the default parameter value of 0.01 for the correlations of genes within gene sets) using gene sets from the curated gene set collection (C2) of the Molecular Signature Database (MSigDB v7.0)

(Subramanian et al., 2005) with a special focus on gene sets from pathway databases, including KEGG (Kanehisa et al., 2017), Biocarta (http://cgap.nci.nih.gov/Pathways/BioCarta_Pathways), PID (Schaefer et al., 2009) and Reactome (Fabregat et al., 2018). We tested a total of 1,576 gene sets containing more than 10 genes and those with a false discovery rate (FDR) lower than 1% were considered significant.

Regulon enrichment analysis

Regulon enrichment analysis was performed similarly to pathway enrichment analysis using camera from the limma package. DoRothEA v2 regulons (Fabregat et al., 2018) were downloaded from <https://github.com/saezlab/DoRothEA>.

More specifically, we used human TOP10score regulons in VIPER format, containing the targets with the highest quality score possible (and at least 10 genes) per transcription factor. Mouse regulons were obtained by orthology: mouse genes with a 1-to-1 or Many-to-1 relationship to human genes of each DoRothEA regulon were obtained using Ensembl Compara (release 97); only orthology relationships annotated to taxonomic levels "Boreoeutheria", "Eutheria", "Euarchontoglires", "Theria", or "Amniota" were retained. We tested a total of 1,307 regulons including at least 10 mouse genes and those with a false discovery rate (FDR) lower than 1% were considered significant.

AGO2 HITS-CLIP (AHC) data

Sample preparation and read depths on seed regions of genes targeted by different miRNA seed families were obtained as previously described (Loeb et al., 2012; Gagnon et al., 2019). Briefly, libraries were constructed using CD4⁺ T cells where nuclei were eliminated. AGO2 immunoprecipitation was performed using a monoclonal antibody (Wako; clone 2D4). Libraries were multiplexed and sequenced on an Illumina HiSeq 2500 system. Reads were binned based on individual barcodes and aligned to the mm10 reference genome using Bowtie (Langmead et al., 2009). Maximum read depths across mature miRNAs and miRNA targets were generated using the samtools package (Li et al., 2009).

In vitro differentiation

T_H1 differentiation conditions were generated with 50U IL-2, 5 ng/mL IL-12 and 10 µg/mL anti-IL-4 per mL T cell medium (Vigne et al., 2011). iT_{reg}s were differentiated with retinoic acid (0.9 mM), 250U IL-2, 0.75 ng/mL TGFβ, 10 µg/mL anti-IFNγ and 10 µg/mL anti-IL-4 (Barrat et al., 2002). T_H17 were generated with 50 ng/mL IL-6, 3 ng/mL TGFβ, 5 µg/mL anti-IFNγ and 10 µg/mL anti-IL-4 per mL T cell medium (Chen et al., 2003). For the differentiation, 2*10⁵ naïve CD4⁺ T cells were plated on a pre-coated 96-well flat bottom plate (coated over night with 0.2 µg anti-CD28, 0.5 µg anti-CD3 per mL PBS) and harvested at 24 h, 48 h or 72 h after plating.

Seahorse

Calibration plates were coated over night with 200 µL calibrant. Cell plates were coated with 18 µL 0.1 M NaHCO₃ pH8.0 6.67% CellTak (Seahorse XF96 flux pack, Bucher Biotech, CH). The following day, cell plates were washed with H₂O and left for drying during cell preparation. Compounds were prepared for a final in-well concentration of 1 µM for Oligomycin, 2 µM for FCCP and 11 µM for Rotenone. CD4⁺ T cells (naïve or activated) were harvested with glucose-free, unbuffered RPMI, washed and counted multiple times before plating 3*10⁵ cells per well. Mitochondrial perturbation was performed by sequential injection of glucose (80 mM stock), oligomycin, FCCP and rotenone. Measurements of oxygen consumption rate (OCR, pMoles/min) and extracellular acidification rate (ECAR; mpH/min) were performed with a Seahorse XF96 flux analyzer (Seahorse Bioscience, USA). Data analysis was performed using Prism (Version7.0d), mitochondrial parameters were calculated as described by Gubser et al. (2013).

Cyclosporin A (CsA) titration

The sensitivity of CD28^{-/-} and rescue cells to compounds interfering with Ca²⁺ signaling was tested. Increasing amounts of CsA were added to the cultures during activation: 2*10⁵ naïve CD4⁺ T cells were plated in 100 µL complete T cell medium in pre-coated 96 well plates. 100 µL of a serial dilution of CsA were then added to result in in-well concentrations of 100 ng/mL, 50 ng/mL, 25 ng/mL, 12.5 ng/mL, 6.5 ng/mL, 3.125 ng/mL, 1.5625 ng/mL or 0 ng/mL. Cells were then activated in the presence of these CsA concentrations for 48 h before harvesting and staining for viability and activation markers.

ImageStream

Naïve CD4⁺ T cells were isolated and activated for 48 h in the presence of 6.25 ng/mL CsA. They were then harvested and washed with PBS before fixation for 20 min at 4°C. Intracellular staining for NFATc2 was performed in a two-step staining with first 1 h at room temperature with anti-NFATc2 in permeabilization buffer, and subsequently 1 h at room temperature with goat anti-mouse IgG1 in permeabilization buffer. Nuclei were stained with DAPI in the last 5 min of incubation. Acquisition was run on an ImageStreamX Mark2 Imaging flow cytometer (Amnis), and data analysis was performed with the IDEAS software (v6.2).

Reverse transcription (RT) and quantitative PCR (qPCR)

5*10⁵ cells were washed resuspend in 400 µL TRIreagent. RNA isolation was then performed according to the isolation protocol from TRIreagent supplier (SIGMA). In brief, 0.1 mL of 1-bromo-3-chloropropane per mL of TRI Reagent was added, samples were mixed by vigorous shaking, incubated for 15 min at room temperature and then centrifuged at 12'000 g for 15 min at 4°C for phase separation. The aqueous phase was then mixed with 0.5 mL of isopropanol per mL of TRI Reagent used, again centrifuged for 10 min for RNA precipitation. RNA was then washed with 70% Ethanol and finally resuspend in RNase-free water. RNA concentration and purity was determined with a Nanodrop2000 Spectrophotometer (ThermoScientific).

For Rcan3 qPCR, reverse transcription was performed using the SIGMA MMLV kit on 1 µg RNA according to the manufacturer's instructions. qPCR was run with TaqMan FAST Universal PCR master mix on an Applied Biosystems® Real-Time PCR System. 18S was used as a reference gene.

For miRNA17 qPCR, reverse transcription was performed using the TaqMan MicroRNA Reverse Transcription Kit (ABI) and a miRNA-specific reverse stem-loop primer according to the manufacturer's instructions (Moltzahn et al., 2011). qPCR was run with TaqMan FAST Universal PCR master mix on an Applied Biosystems® Real-Time PCR System. SNO234 was used as a reference gene.

CRISPR/Cas9 editing of naïve CD4⁺ T cells

Protospacer sequences were taken from the Brie library (Doench et al., 2016) and ordered as CRISPR RNAs (crRNAs) from IDT. Cas9 ribonucleoproteins (RNPs) were prepared as described (Dolz et al., 2021). During preparation, 1.44 µL of 100 mg/mL of poly-L-glutamic acid (PGA) solution (Sigma) was added to gRNAs to improve cutting efficiency (Nguyen et al., 2020).

Naïve CD4⁺ T cells were isolated from CD28^{-/-} mice as described above, labelled with CTV and cultured for 24 h in 24-well plates at a density of 3*10⁶/mL in T cell medium supplemented with 5 ng/mL IL-7. Prior to electroporation, 1.8–2*10⁶ cells/electroporation were washed with PBS, counted and resuspended in 20 µL P4 buffer (Lonza). Cells were electroporated with Lonza Nucleofector 4D in 16-well strips using pulse code DS137. After electroporation, cells were cultured in IL-7 supplemented medium for 5 days and activated with plate-bound anti-CD3/anti-CD28 as described above for low stimulation, i.e. 0.2 µg anti-CD28, 0.5 µg anti-CD3 per mL PBS. Cells were harvested and stained for flow cytometry after 48 and 72 hours of activation. Leftover naïve cells were washed with PBS, resuspended in QuickExtract solution (Lucigen), vortexed for 1 min, incubated at 60°C for 6 minutes, vortexed for 1 min and incubated at 98°C for 10 minutes to extract genomic DNA. Genomic DNA was used for PCRs that were sequenced to measure editing efficiency using TIDE (<https://tide.nki.nl/>).

QUANTIFICATION AND STATISTICAL ANALYSIS

Statistical analysis was performed with GraphPad Prism (v7.0d, Graphpad Software). Normal distribution was not assumed, and non-parametric tests were chosen individually depending on the type of experiment as indicated in the figure legends. The overall statistical significance was set to 5% ($\alpha = 0.05$), and error bars represent standard deviation (SD). N corresponds to number of biological replicates. We used Kruskal-Wallis tests for most of the experiments with more than two unpaired groups and one factor (e.g., %Fas⁺ GL7⁺ population in three genotypes), followed by Dunn's multiple comparison test or Dunnett's multiple comparison test for CRISPR experiments. We used two-way Anova for experiments including two factors (e.g., %CD44^{hi}CD62^{lo} population in three genotypes activated with or without anti-CD28), followed by Tukey's multiple comparison test.